Casson fluid Performance on MHD Radiating and Rotating Flow Past a Vertically Inclined Plate Including Hall Effect and Cross Diffusion

Ch. Krishna Sagar[*] and G. Srinivas

[*]*Department of Mathematics, Visvesvarya College of Engineering and Technology, Ibrahimpatnam, Hyderabad, Telangana State.*

[1]*Department of Mathematics, Gurunanak Institute of Technology, Ibrahimpatnam, Hyderabad, Telangana State, India.*

Abstract: *In the presence of chemical reaction, heat transfer and mass transfer, the combined effects of the Hall current and the thermal radiation on the magnetic fluid flow of a time-varying magnetic fluid on a vertically inclined porous plate were investigated. The fluid flow model is constructed as a set of differential equations which are non-linear partial. Instead of partial derivatives linear the non-dimensional quantities are used to obtain a series of ordinary linear coupled partial differential equations. In addition, the numerical method, that is, finite difference method is used to solve the governing the differential equations. Perform a detailed parametric analysis to verify the effects of several important parameters, such as Casson flow parameters, Hall parameter, Magnetic field parameter, Thermal radiation parameter, etc. on the contours of velocity, temperature and concentration fields. The behaviours of the new quantities of engineering interest is also discussed, such as skin-friction, heat and mass transfer rate and the speed of the material exchange coefficient. The fluid flow problems presented in this research work can be applied to suspensions of silicon, blood flow, polymer spheres and the printing industry.*

Keywords: *Casson fluid; MHD; Rotation; Thermal radiation; Hall Effect; Finite difference method;*

1. Introduction:

Since a single model cannot describe all the properties of a fluid, it is essential to study the flow problems in a vertical plate through various combinations. In the literature, non-Newtonian fluid phenomena require much attention due to their wide range of applications. In 1995, Casson introduced a fluid flow model associated with non-Newtonian fluid flow. Among all non-Newtonian fluid models, the Casson fluid model is one of the most important models for revealing performance stress characteristics. The Casson fluid model is based on the interaction of solid and liquid phases. When the yield stress is more important than the shear stress, the Casson fluid acts as a solid. On the other hand, when the yield stress is less than the cutting voltage, it starts to move. Chili sauce, honey, jelly, condensed milk and blood are some examples of Casson fluids. The Casson flquid flow model can also be used for the treatment of cancer. Eldabe and Salwa [1] studied for the first time the Casson fluid flow between two coaxial cylinders. It took many years to get the most out of this phenomenon. Shehzad et al. [2] taking into account the effects of chemical reactions and inhalation, the transfer of heat and mass in non-magnetic fluids was investigated.

Tufail et al. [3] studied the effect of the heat source/sink on the magnetohydrodynamic fluid flow and the heat transfer on the porous traction surface was analyzed. Nandy [4] studied the effect of the partial slip velocity of the Casson MHD fluid flowing along the stretched surface. He got a solution to the point of stagnation. Mukhopadhyay [5] studied the heat transfer phenomenon of the MHD Casson fluid that flows along the elongated plate. Vajravelu et al. [6] studied the flow and heat transfer of Casson fluids due to permeable index surfaces. Mukhopadhyay and Vajravelu [7] studied the instability of Casson's fluid on porous surfaces. The theoretical studies of entropy generation in constant laminar flow of Casson nanofluids, including the effects of velocity and convective boundary conditions, were carried out by Abolbashari et al. [8]. It has been found that as the Casson parameter decreases, entropy generation increases. Ashraf et al. [9] studied the mixed convection of Casson's fluids along the strecthed surface in the presence of the Hall effect. Butt et al. [10] studied the three-dimensional problem of Casson's fluid flow along unstable stress surfaces. Khan and others. [11] studied the homogenous-heterogeneous reaction of the Casson fluid. Seth et al. Considered the effect of viscosity and Ohmic dissipation on the unsteady MHD flow of Casson fluid in horizontally extendable sheets in non-Darcy porous media.[12]

It is well known that in the case of a conductive fluid that flows under the influence of a magnetic field, the secondary flow is induced by the secondary flow due to the Hall effect that occurs after the strong magnetic field. And the density of the fluid is low. The Hall effect has several implications in the determination of the flow characteristics in a flow field. Therefore, some authors have theoretically studied the effect of Hall current on the magnetohydrodynamic flow of viscous, incompressible and conductive fluids. Gupta [13] studied the effect of the Hall current along a permeable surface in liquid magnetic fluids. Chamkha [14] studied the effect of Hall current on the natural hydromagnetic convection of viscous and conductive fluids in porous media. Takhar et al. [15] proposes a solution not similar to the flux of the boundary layer of the conductive fluid on the moving surface in the presence of a magnetic field and the effect of the Hall current. Hayat et al. [16] studied the effects of heat transfer and Hall current on the permeable surface in a second-order rotating fluid stream. Saleem and Aziz [17] studied the combined effects of hall current and the diffusion of mass in the laminar flow of the fluids of absorption/fluids of magnetic fluids. Seth et al. ([18] and [19]) taking into account the effects of Hall current, heat absorption and heat radiation, the exact results of the unsteady hydromagnetic convection heat and mass transfer flow in media are presented porous region. Hussain [20] and others studied the effects of Hall current and heat absorption on natural convection caused by accelerated plates in the presence of chemical reaction. Pal [21] analyzed the combined effects of the Hall current and the heat transfer by radiation in the time-dependent magnetic fluid flow along the porous surface. Jain and Chaudhary [22] presented the Hall effect of magnetohydrodynamic convection of viscoelastic fluids in infinitely vertical

perforated plates by mass and radiation transfer. Satya Narayana et al. [23] studied the effect of Hall current and radiation on the absorption of porous MHD fluids in a rotating system. In Sarma and Pandit [24], the authors studied the effects of hall current, rotation and Soret on infinite vertical plates incorporated into porous media, heat transfer by convection and transfer of mass by convection of non-fluid and non-compressive MHD. conductive fluids.

So the aim of our work is to extend the work of Sarma and Pandit [24], including Dufour, Casson fluid and Angle of inclination effects. As far as we know, the Hall current has had little work on the effects of the chemically reactive magnetohydrodynamics in Casson fluid flow, which combines the rotational effects of the flow in the presence of heat and mass transfer. The problem of governing the limit value is solved numerically by the finite difference method. The effects of various physical parameters on the primary velocity, the secondary velocity, the temperature and concentration profiles, the coefficient of skin-friction, the Sherwood number and the Nusselt number are shown in the tabular forms. Finally, a qualitative verification of the analysis is carried out comparing the current results with previously published works. This result is consistent with the verification of the physical reality of the precision of our work presented here.

2. Formation of Flow Governing Equations:

Consider the mass of the non-stationary natural convection MHD with heat transfer and the incompressible conductive fluid in an infinite vertical plate combined in a uniform porous medium in a rotating system, which takes into account the Hall current. A very interesting fact is that the effect of the Hall current produces a force in the z' - direction, which in turn produces a lateral flow velocity in this direction, so the flow becomes three-dimensional. The geometry of the problem is shown in Figure 1.For this survey, make the following assumptions:

i. Assuming that the Hall current, Ohm's generalized law [25] can take the following form:

$$\vec{J} = \frac{\sigma}{1+m^2}\left(\vec{E} + \left(\vec{V} \times \vec{B}\right) - \frac{1}{\sigma n_e}\left(\vec{J} \times \vec{B}\right)\right) \quad (1)$$

ii. Coordinate system is chosen in such a way that x'-axis is considered along the plate in upward direction and y'-axis normal to plane of the plate in the fluid.

iii. A uniform transverse magnetic field B_0 is applied in a direction which is parallel to y'-axis.

iv. The fluid and plate rotate in unison with uniform angular velocity x' about y'-axis.

v. Initially i.e., at time $t' \leq 0$, both the fluid and plate are at rest and are maintained at a uniform temperature T'_∞.

vi. Also species concentration at the surface of the plate as well as at every point within the fluid is maintained at uniform concentration C'_∞.

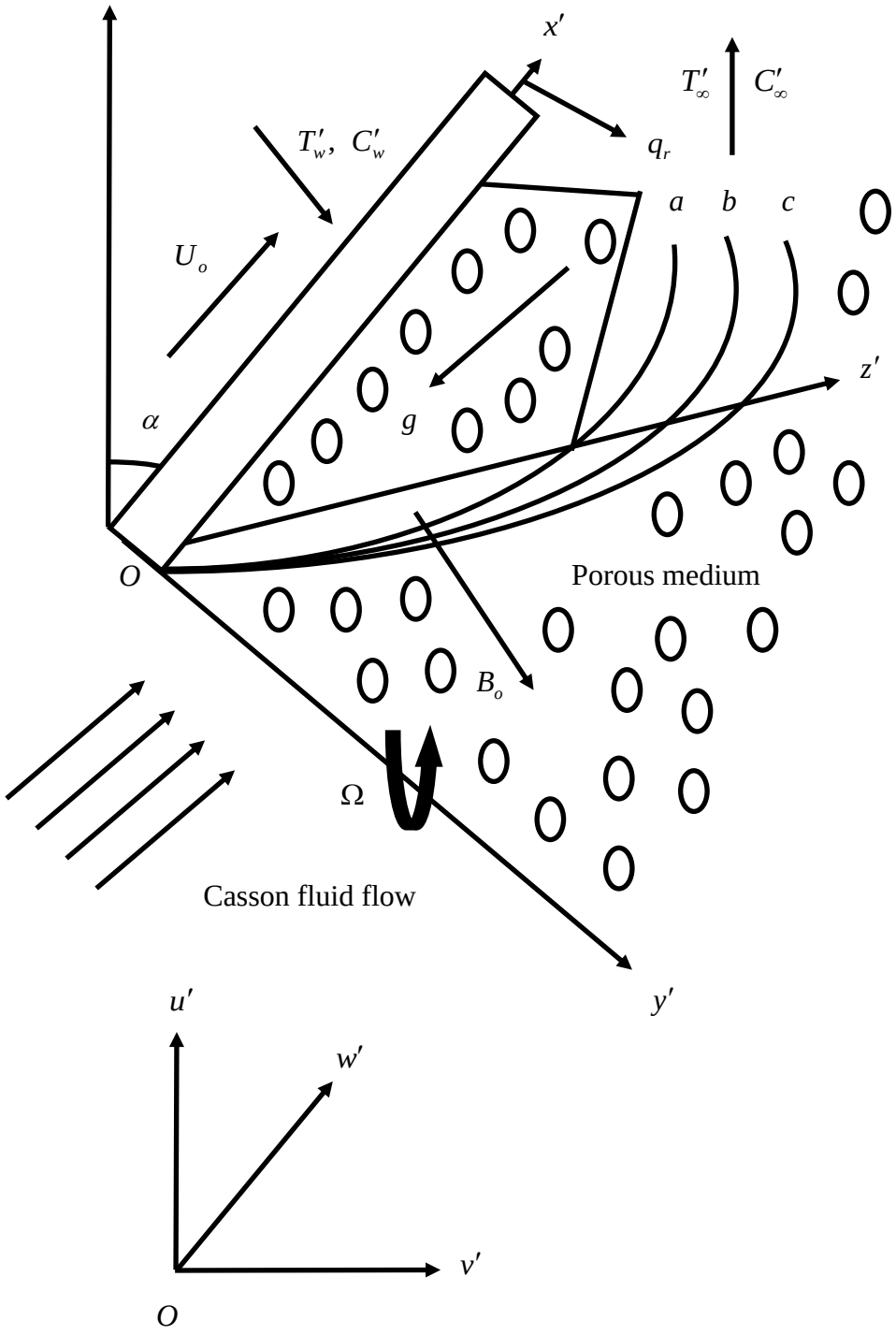

a --- Momentum boundary layer, *b* --- Thermal boundary layer, *c* --- Concentration boundary layer

Fig. 1. Geometry of the problem

vii. At time $t' > 0$, plate starts moving in x'-direction with a velocity $u' = Ut'$ in its own plane.

viii. The temperature at the surface of the plate is raised to uniform temperature T_w' and species concentration at the surface of the plate is raised to uniform species concentration C_w' and is maintained thereafter.

ix. Since plate is of infinite extent in x' and z' directions and is electrically non-conducting, all physical quantities except pressure depend on y' and t' only.

x. In addition, there is no applied or polarized voltage, so the polarization effect of the fluid is negligible. This corresponds to the case in which the electrical device adds or extracts energy from the fluid [26].

xi. It is assumed that the induced magnetic field generated by the fluid flow is negligible compared to that applied. This assumption is reasonable because the Reynolds number of liquid metal and partially ionized liquid is very small and these liquids are commonly used in industrial applications [26].

xii. The Cauchy stress tensor, $\bar{S}$ of a Casson's non-Newtonian fluid [27] takes the form as follows:

$$\bar{S} = \frac{\mu}{1+\lambda}\left(\dot{\lambda} + \lambda_1 \ddot{\lambda}\right) \tag{2}$$

Where μ is the dynamic viscosity, λ_1 is the ratio of relaxation to retardation times, dot above a quantity denotes the material time derivative and λ is the shear rate. The Casson model provides an elegant formulation that simulates the effects of retardation and relaxation that occur in non-Newtonian polymer streams. The cutting rate and the cutting velocity gradient are defined in more detail according to the velocity vector, $\bar{V}$, as follows:

where $\dot{\lambda} = \nabla\bar{V} + (\nabla\bar{V})^T$ (3)

and $\ddot{\lambda} = \frac{d}{dt}\left(\dot{\lambda}\right) + (\bar{V}.\nabla)\dot{\lambda}$ (4)

Taking into account the assumptions presented above, it regulates the free convection equation of the Casson flow by heat transfer and mass transfer of the incompressible conductive fluid, and is incorporated into the uniform porous medium in the system by means of a vertically inclined plate. The rotation considering the Hall current and the cross-diffusion effects is given by

Momentum Equation:

$$\frac{\partial u'}{\partial t'} + 2\Omega' w' = \nu\left(1+\frac{1}{\gamma}\right)\frac{\partial^2 u'}{\partial y'^2} - \frac{\sigma B_o^2}{\rho(1+m^2)}(u' + mw') + g\beta(T' - T'_\infty)(\cos\alpha) + g\beta^*(C' - C'_\infty)(\cos\alpha) - \left(\frac{\nu}{K'}\right)u' \tag{5}$$

$$\frac{\partial w'}{\partial t'} - 2\Omega' u' = \nu\left(1+\frac{1}{\gamma}\right)\frac{\partial^2 w'}{\partial y'^2} + \frac{\sigma B_o^2}{\rho(1+m^2)}(mu' - w') - \left(\frac{\nu}{K'}\right)w' \tag{6}$$

Energy Equation:

$$\frac{\partial T'}{\partial t'} = \left(\frac{\kappa}{\rho C_p}\right)\frac{\partial^2 T'}{\partial y'^2} - \frac{1}{\rho C_p}\frac{\partial q_r}{\partial y'} + \left(\frac{D_m k_T}{\rho C_p C_s}\right)\frac{\partial^2 C'}{\partial y'^2} \tag{7}$$

Concentration Equation:

$$\frac{\partial C'}{\partial t'} = D\frac{\partial^2 C'}{\partial y'^2} + \left(\frac{D_m k_T}{T_m}\right)\frac{\partial^2 T'}{\partial y'^2} - K_r'(C' - C_\infty') \tag{8}$$

Initial and boundary conditions for the fluid flow problem are given below:

$$\left.\begin{aligned} t' \le 0:\ & u' = 0,\quad w' = 0,\ T' = T_\infty',\ C' = C_\infty' \quad for\ all \quad y' \\ t' > 0: & \begin{cases} u' = Ut',\ w' = 0,\ T' = T_w',\ C' = C_w' & at \quad y' = 0 \\ u' \to 0,\ w' \to 0,\ T' \to T_\infty',\ C' \to C_\infty' & as \quad y' \to \infty \end{cases} \end{aligned}\right\} \tag{9}$$

For an optically thick fluid, in addition to emission there is also self absorption and usually the absorption coefficient is wavelength dependent and large so we can adopt the Rosseland approximation for the radiative heat flux vector q_r. Thus q_r is given by

$$\frac{\partial q_r}{\partial y'} = -\frac{4\sigma^*}{3k_1}\left(\frac{\partial T'^4}{\partial y'}\right) \tag{10}$$

Where σ^* is the Stefan-Boltzmann Constant and k_1 is the Rosseland mean absorption coefficient. We assume that the temperature differences within the flow are sufficiently small so that T'^4 can be expressed as a linear function. By using Taylor's series, we expand T'^4 in Taylor series about T_∞' which after neglecting higher order terms takes the form:

$$T'^4 \cong T_\infty'^4 + 4(T' - T_\infty')T_\infty'^3 = 4T'T_\infty'^3 - 3T_\infty'^4 \tag{11}$$

Eq. (7) with the help of (10) and (11) reduces to

$$\frac{\partial T'}{\partial t'} = \left(\frac{\kappa}{\rho C_p}\right)\frac{\partial^2 T'}{\partial y'^2} - \left(\frac{16\sigma^* T_\infty'^3}{3k_1\rho C_p}\right)\frac{\partial^2 T'}{\partial y'^2} + \left(\frac{D_m k_T}{\rho C_p C_s}\right)\frac{\partial^2 C'}{\partial y'^2} \tag{12}$$

Introducing the following non-dimensional quantities:

$$\left.\begin{aligned} & u = \frac{u'}{U_o},\ y = \frac{y'U_o}{\nu},\ t = \frac{t'U_o^2}{\nu},\ w = \frac{w'}{U_o},\ \theta = \frac{T' - T_\infty'}{T_w' - T_\infty'},\ \phi = \frac{C' - C_\infty'}{C_w' - C_\infty'},\ K = \frac{K'U_o^2}{\nu^2},\ \mathrm{Pr} = \frac{\rho\nu C_p}{\kappa}, \\ & Sc = \frac{\nu}{D},\ M^2 = \frac{\sigma\nu B_o^2}{\rho U_o^2},\ Gr = \frac{\nu g\beta(T_w' - T_\infty')}{U_o^3},\ Gc = \frac{\nu g\beta(C_w' - C_\infty')}{U_o^3},\ Kr = \frac{K_r'\nu}{U_o^2},\ N = \frac{\kappa k_1}{4\sigma^* T_\infty'^3}, \\ & Sr = \frac{D_m k_T(T_w' - T_\infty')}{\nu T_m(C_w' - C_\infty')},\ Du = \frac{D_m k_T(C_w' - C_\infty')}{\nu\rho C_S C_p(T_w' - T_\infty')},\ \Omega = \frac{\nu\Omega'}{U_o^2},\ U = \frac{U_o^3}{\nu} \end{aligned}\right\} \tag{13}$$

Eqs. (5), (6), (8) and (12) in non-dimensional form are given below:

Momentum Equation:

$$\frac{\partial u}{\partial t} + 2\Omega w = \left(1 + \frac{1}{\gamma}\right)\frac{\partial^2 u}{\partial y^2} - \frac{M^2}{(1+m^2)}(u + mw) + Gr\theta(\cos\alpha) + Gc\phi(\cos\alpha) - \frac{u}{K} \tag{14}$$

$$\frac{\partial w}{\partial t} - 2\Omega u = \left(1 + \frac{1}{\gamma}\right)\frac{\partial^2 w}{\partial y^2} + \frac{M^2}{(1+m^2)}(mu - w) - \frac{w}{K} \tag{15}$$

Energy Equation:

$$\frac{\partial \theta}{\partial t} = \frac{1}{\Pr}\left(\frac{3N+4}{3N}\right)\frac{\partial^2 \theta}{\partial y^2} + (Du)\frac{\partial^2 \phi}{\partial y^2} \tag{16}$$

Concentration Equation:

$$\frac{\partial \phi}{\partial t} = \frac{1}{Sc}\frac{\partial^2 \phi}{\partial y^2} + (Sr)\frac{\partial^2 \theta}{\partial y^2} - Kr\phi \tag{17}$$

The relevant initial and boundary conditions in non-dimensional form are given by:

$$\left.\begin{array}{l} t \le 0: \quad u = 0, \quad w = 0, \quad \theta = 0, \quad \phi = 0 \quad for\ all \quad y \\ t > 0: \begin{cases} u = t, \quad w = 0, \quad \theta = 1, \quad \phi = 1 \quad at \quad y = 0 \\ u \to 0, \quad w \to 0, \ \theta \to 0, \ \phi \to 0 \quad as \quad y \to \infty \end{cases} \end{array}\right\} \tag{18}$$

For the practical application of the engineering and design of chemical engineering systems, the local skin-friction coefficients (due to the primary and secondary velocity), the coefficients of Nusselt numbers and the Sherwood numbers are important physical parameters of this flow. Limitation The coefficient of friction of the surface due to the primary velocity and the secondary velocity distributions at the plate, which is given by the following equation in the dimensionless form

$$Cf_1 = \left(1 + \frac{1}{\lambda}\right)\frac{\tau'_x}{\rho U_o \nu} = \left(1 + \frac{1}{\gamma}\right)\left(\frac{\partial u}{\partial y}\right)_{y=0} \tag{19}$$

$$Cf_2 = \left(1 + \frac{1}{\lambda}\right)\frac{\tau'_z}{\rho U_o \nu} = \left(1 + \frac{1}{\gamma}\right)\left(\frac{\partial w}{\partial y}\right)_{y=0} \tag{20}$$

The rate of heat transfer coefficient, which in the non-dimensional form in terms of the Nusselt number is given by $Nu = -x'\dfrac{\left(\dfrac{\partial T'}{\partial y'}\right)_{y'=0}}{T'_w - T'_\infty} \Rightarrow Nu\,\mathrm{Re}^{-1} = -\left(\dfrac{\partial \theta}{\partial y}\right)_{y=0}$ (21)

The rate of mass transfer coefficient, which in the non-dimensional form in terms of the Sherwood number, is given by $Sh = -x'\dfrac{\left(\dfrac{\partial C'}{\partial y'}\right)_{y'=0}}{C'_w - C'_\infty} \Rightarrow Sh\,\mathrm{Re}^{-1} = -\left(\dfrac{\partial \phi}{\partial y}\right)_{y=0}$ (22)

Where $\mathrm{Re} = \dfrac{U_o x'}{\nu}$ is the local Reynolds number.

3. Finite Difference Technique Solutions:

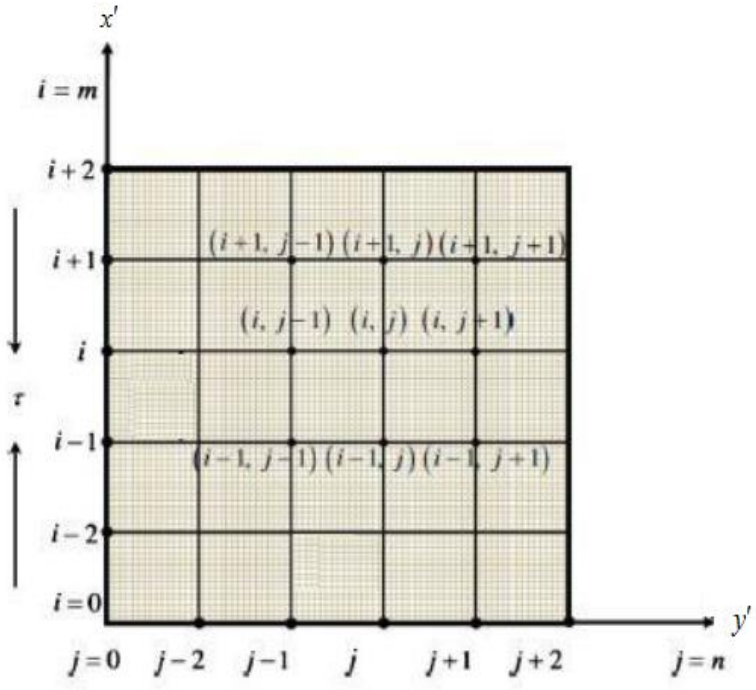

Fig. 2. Finite difference space grid

The non-linear momentum, energy and concentration equations given in equations (14), (15), (16) and (17) are solved under the appropriate initial and boundary conditions (18) by the implicit finite difference method. The transport equations (14), (15), (16) and (17) at the grid point (i, j) are expressed in difference form using Taylor's expansion:

$$\left(\frac{u_i^{j+1}-u_i^j}{\Delta t}\right)+2\Omega w_i^j=\left(1+\frac{1}{\gamma}\right)\left(\frac{u_{i+1}^j-2u_i^j+u_{i-1}^j}{(\Delta y)^2}\right)-\frac{M^2}{(1+m^2)}\left(u_i^j+mw_i^j\right)$$
$$+(Gr)(\cos\alpha)\theta_i^j+(Gc)(\cos\alpha)\phi_i^j-\frac{u_i^j}{K} \quad (23)$$

$$\left(\frac{w_i^{j+1}-w_i^j}{\Delta t}\right)-2\Omega u_i^j=\left(1+\frac{1}{\gamma}\right)\left(\frac{w_{i+1}^j-2w_i^j+w_{i-1}^j}{(\Delta y)^2}\right)+\frac{M^2}{(1+m^2)}\left(mu_i^j-w_i^j\right)-\frac{w_i^j}{K} \quad (24)$$

$$\left(\frac{\theta_i^{j+1}-\theta_i^j}{\Delta t}\right)=\frac{1}{\Pr}\left(\frac{3N+4}{3N}\right)\left(\frac{\theta_{i+1}^j-2\theta_i^j+\theta_{i-1}^j}{(\Delta y)^2}\right)+(Du)\left(\frac{\phi_{i+1}^j-2\phi_i^j+\phi_{i-1}^j}{(\Delta y)^2}\right) \quad (25)$$

$$\left(\frac{\phi_i^{j+1}-\phi_i^j}{\Delta t}\right)=\frac{1}{Sc}\left(\frac{\phi_{i+1}^j-2\phi_i^j+\phi_{i-1}^j}{(\Delta y)^2}\right)+(Sr)\left(\frac{\theta_{i+1}^j-2\theta_i^j+\theta_{i-1}^j}{(\Delta y)^2}\right)-Kr\phi_i^j \quad (26)$$

Where the indices i and j refer to y and t respectively. The initial and boundary conditions (18) yield

$$\left.\begin{aligned}&u_i^0=0,\ w_i^0=0,\ \theta_i^0=0,\ \phi_i^0=0\ \ for\ all\ i,\\&u_i^j=t,\ w_i^0=0,\ \theta_i^j=1,\ \phi_i^j=1\ at\ i=0\\&\&\ u_M^j\to 0,\ w_M^j\to 0,\ \theta_M^j\to 0,\ \phi_M^j\to 0\end{aligned}\right\} \quad (27)$$

Thus the values of u, w, θ and ϕ at grid point $t = 0$ are known; hence the temperature field has been solved at time $t_{i+1} = t_i + \Delta t$ using the known values of the previous time $t = t_i$ for all $i = 1, 2, ..., N-1$. Then the velocity field is evaluated using the already known values of temperature and concentration fields obtained at $t_{i+1} = t_i + \Delta t$. These processes are repeated till the required solution of u, w, θ and ϕ is gained at convergence criteria:

$$abs\left|(u,\ w,\ \theta,\ \phi)_{exact} - (u,\ w,\ \theta,\ \phi)_{numerical}\right| < 10^{-3} \quad (28)$$

4. Results And Discussions:

Study of the oscillating sheet in a perpendicular direction Casson fluid unstable hydromagnetotherapy radiation flow in a non-linear numerical manner, comprising a stream Corridor , magnetic thermal diffusion, the influence of thermal diffusion. The fluid flow pattern is performed on behalf of a group of differential equations derived partially dependent on time and so linear space. These partial differential equations processed by numerical methods are finite difference methods for solving differential equations. The results of the calculation indicate the relevant impact flow parameters, such as the Grashof number for heat transfer (Gr), Grashof number for mass transfer (Gc), Magnetic field parameter (M^2), Permeability parameter (K), Hall parameter (m), Prandtl number (Pr), Schmidt number (Sc), Angle of inclination parameter (α), Casson fluid parameter (γ), Rotation parameter (Ω), Thermal radiation parameter (N), Dufour number or diffusion thermo parameter (Du), Soret number or thermal diffusion parameter (Sr), Chemical reaction parameter (Kr) and time (t). To investigate the implications of non-dimensional parameters on the skin-friction coefficients, local Nusselt number and local Sherwood number the numerical values of Cf_1, Cf_2, Nu and Sh for different values of the parameters are presented and discussed in tabular forms. For computational purpose the default parameter values are taken as $Gr = 1.0$, $Gc = 1.0$, $M^2 = 0.5$, $m = 0.5$, $K = 0.5$, Pr = 0.71, $Sc = 0.22$, $\alpha = 45^o$, $\gamma = 0.5$, $\Omega = 0.5$, $N = 0.5$, $Du = 0.5$, $Sr = 0.5$, $Kr = 0.5$ and $t = 1.0$.

- Figs. 3 to 6 show the effect of the concentration of the thermal flotation forces and the velocity of the primary and secondary fluid. As can be seen in Fig. 3, the velocity of the primary fluid u increases as Gr increases in the vicinity of the plate surface and decreases as Gr increases in the region away from the plate. As can be seen in Fig. 4, the velocity of the secondary fluid w decreases as the Gr increases in the entire region of the boundary layer. Of the Figs. 5 and 6 show that u and w increase as Gc increases. Gr represents the relative strength of the thermal buoyancy with respect to the viscous force, and Gc represents the relative strength of the buoyancy of the concentration with respect to the viscous force. Therefore, as the intensity of the thermal buoyancy increases, Gr decreases and as the

buoyancy of the concentration increases, *Gc* increases. In this problem, the natural convection caused by the floating forces and thermal concentration, therefore, the thermal flotation tends to slow down the primary and secondary fluids, while the floating force of the concentration tends to accelerate the primary in the entire region of the boundary layer. And the speed of the secondary fluid, which is clearly seen in Figs. 3-6.

- Figs. 7 and 8 show velocity *u* of the primary and secondary velocity on the effect of the Hall current of *w*. It is perceived by figures 1 and 2. As shown in Figures 7 and 8, the primary velocity *u* decreases as the *m* increases in the entire region of the boundary layer, and the secondary velocity w increases as the *m* increases in the entire region of the layer limit .This means that the Hall current tends to accelerate the velocity of the secondary fluid throughout the region of the boundary layer, which is consistent with the fact that the Hall current causes a secondary flow in the flow field, while counter current. speed. The main fluid in the entire area of the boundary layer.
- Figures 9 and 10 illustrate the rotation effect (Ω) of the primary and secondary fluid velocity. It is obvious from Figs. 9 and 10, the primary speed *u* decreases with the increase Ω, and the secondary velocity *w* increases as you move away from the plate in the Ohm region increases. This means that the rotation delays the flow of the fluid in the principal direction of the flow and accelerates the flow of the flow in the secondary direction of the flow in the region of the boundary layer. This can be attributed to the fact that when the friction layer in the moving plate is suddenly inserted in the movement, the Coriolis force acts as a restriction of the main fluid flow, that is, a cross flow occurs in the flow of fluid or in the direction of the main flow. That is, secondary flow.
- Schmidt number (*Sc*) in the primary velocity, the secondary velocity and the concentration distribution is shown in Figs. 11, 12 and 13, respectively. In Figs. 11, 12 and 13, *u* , *w* and φ decrease as *Sc* increases. The Schmidt number represents the relationship between the moment and the mass diffusion coefficients. Schmidt's number then quantifies the relative validity of the momentum and mass transfer through the diffusion in the boundary layers of fluid dynamics (velocity) and concentration (species). As the number of Schmidt increases, the concentration decreases. This results in a decrease in the buoyancy effect of the concentration, which results in a decrease in fluid velocity. The reduction of the velocity and concentration curves is accompanied by a simultaneous decrease in the velocity and concentration limiting layers .These behaviours can be clearly seen in the Figs. 11, 12 and 13.
- Figs. 14 and 15 show the effect of the porous medium (*K*) primary and secondary permeability to the fluid velocity. As shown in Figs. 14 and 15, with the important parameter increasing the velocity of the permeability decreases, while its velocity has a secondary

reaction. It is evident from the flow configuration that an increase in the porosity of the medium contributes to the flow in the secondary direction, thus increasing the secondary velocity due to its orientation through the porous medium.

- Figs. 16 and 17 illustrate the effect of the chemical reaction of the parameters *Kr* velocity of the primary fluid (*u*) and a secondary fluid velocity (*w*). It can be seen that an increase in the chemical reaction parameter (*Kr*) leads to an increase in the thickness of the speed boundary layer, indicating that the chemical reaction (*Kr*) can greatly change the diffusion rate. For the increase in the value of *Kr*, the maximum time range of the velocity distribution is clearly seen. It must be remembered here that the positive physical value of *Kr* means a destructive reaction while the negative value of chemical reaction *Kr*. We study the case of destructive chemical reactions (*Kr*).
- Figs. 18, 19 and 20 show an effect of thermal radiation (*N*) on the primary velocity, the secondary fluid temperature and the fluid velocity. In Figs. 18, 19 and 20, the thermal radiation of the door is reduced at each velocity and temperature. Physically, thermal radiation causes a decrease in the temperature of the fluid medium and, therefore, a decrease in the kinetic energy of the fluid particles. This results in a corresponding decrease in fluid velocity. Therefore, the Figs. 18, 19 and 20 are in good agreement with the laws of physics. So with the increase of *N*, θ, *u* and *w* will be reduced. Now, from these figures it can be inferred that the effect of radiation on temperature is greater than the effect on velocity. Therefore, thermal radiation does not have a significant effect on velocity, but it has a relatively more pronounced effect on the temperature of the mixture.
- Figs. 21 and 22 display the influence of Soret number on primary and secondary fluid velocities. It is evident from Figs. 21 and 22 that *u* and *w* increase on increasing Soret number *Sr*. This implies that Soret number tends to accelerate primary and secondary fluid velocities throughout the boundary layer region. Increasing Soret number indicates a fall in the viscosity of the mixture. This leads to increased inertia effects and diminished viscous effects. Consequently the velocity components increase.
- Figs. 23 and 24 show the effect of the time of the primary and secondary fluid velocity (*t*). It is obvious from Figs. 23 and 24 where *u* and *w* increase as *t* increases. This means that the speed of primary and secondary fluids accelerates as time develops in the boundary layer region.
- The numerical values of fluid temperature (θ) are displayed graphically versus boundary layer co-ordinate *y* in Figs. 25 and 26 for various values of Prandtl number (Pr) and time (*t*). It is evident from Fig. 25 that, fluid temperature decreases on increasing Pr. An increase in Prandtl number reduces the thermal boundary layer thickness. Prandtl number signifies the ratio of

momentum diffusivity to thermal diffusivity. It can be noticed that as Pr decreases, the thickness of the thermal boundary layer becomes greater than the thickness of the velocity boundary layer according to the well-known relation $\delta T / \delta \cong 1/\Pr$ where δT the thickness of the thermal boundary layer and δ the thickness of the velocity boundary layer, so the thickness of the thermal boundary layer increases as Prandtl number decreases and hence temperature profile decreases with increase in Prandtl number. In heat transfer problems, the Prandtl number controls the relative thickening of momentum and thermal boundary layers. When Prandtl number is small, it means that heat diffuses quickly compared to the velocity (momentum), which means that for liquid metals, the thickness of the thermal boundary layer is much bigger than the momentum boundary layer. Hence Prandtl number can be used to increase the rate of cooling in conducting flows. Fig. 26 shows that fluid temperature increases on increasing time (*t*). This implies that, there is an enhancement in fluid temperature with the progress of time throughout the thermal boundary layer region.

- Figs. 27-29 show the effects of Chemical reaction (*Kr*), Thermal diffusion parameter (*Sr*) and time (*t*) of the various values. Fig. 27 shows the effect of chemical reactions on the distribution of concentration. In this study, we are analyzing the effects of destructive chemical reactions ($Kr > 0$). It should be noted that as the chemical reaction increases, the concentration profiles decreases. Physically, due to destructive conditions, the chemical reaction has caused many interferences. This in turn leads to the movement of the polymer, which results in an increase in transport phenomena, which reduces the distribution of the concentration in the fluid flow. It is observed in Fig. 28 that the concentration of the substance increases as the number of Soret (*Sr*) increases. An increase in the Soret effect indicates the diffusivity of the molar mass, as indicated by the definition of *Sr*. An increase in the diffusion rate of the molecular weight increases the concentration. This means that the number of Soret tends to increase the concentration of fluid species. As is clear from Fig. 29, as the mass diffuses without remaining in the fluid stream, the molar concentration of the mixture increases with time, so that the concentration of the species increases with time.
- As shown in Figs. 30 and 31, when the magnetic field increases the parameter (M^2), the primary and secondary rapid decrease. This is because when a magnetic field is applied, then origin of the force of Lorentz is opposite to the flow, so the primary and secondary velocities are reduced.
- Figs. 32 and 33 show the effect on the Dufour number on primary and secondary distributions. As the number of Dufour parameter increases, the primary and secondary fluid velocity increases exponentially throughout the region. Figure 34 shows the effect of the

Dufour number on the temperature profile. As the number of Dufour increases, the temperature increases throughout the boundary region.

- The effect of angle of inclination to the vertical direction on the velocity is shown in Fig. 35. From this figure we observe that the velocity is decreased by increasing the angle of inclination due to the fact that as the angle of inclination increases the effect of the buoyancy force due to thermal diffusion decreases by a factor of $\cos\alpha$. Consequently, the driving force to the fluid decreases as a result there is decrease in the velocity profile. Further, it is observed that the combined effects of suction and the buoyancy force (maximum for $\alpha = 0$) overshoots the main stream velocity significantly.
- From Figs. 36 and 37, we observe that as Pr increases, primary velocity profiles and secondary velocity profiles decrease respectively. This happens because when Pr increases the thermal boundary layer thickness rapidly decreases. This causes an increase in fluid viscosity. Consequently the primary velocity profiles and secondary velocity profiles decrease
- The influence of Casson parameter (γ) on the profiles of fluid velocity in x'-direction (primary velocity) and z'-directions (secondary velocity) are shown graphically in Figs. 38 and 39 respectively. It is evident from these figures that on increasing the values of both Casson parameter, the fluid flow velocities (primary velocity and secondary velocity) decreases within the boundary layer region. The Casson parameter measures the yield stress and when it becomes large, the fluid behaves as a Newtonian fluid. The increase in the yield stress causes a stabilization effect.
- The influence of Grashof number for heat transfer (Gr), Grashof number for mass transfer (Gc), Magnetic field parameter (M^2), Permeability parameter (K), Hall parameter (m), Prandtl number (Pr), Schmidt number (Sc), Angle of inclination parameter (α), Casson fluid parameter (γ), Rotation parameter (Ω), Thermal radiation parameter (N), Dufour number or diffusion thermo parameter (Du), Soret number or thermal diffusion parameter (Sr), Chemical reaction parameter (Kr) and time (t) on skin-friction coefficient (Cf_1) due to primary velocity profiles is discussed in tables 1, 2 and 3. From these tables, we observed that the skin-friction coefficient is increasing with increasing values of Grashof number for heat transfer (Gr), Grashof number for mass transfer (Gc), Dufour number or diffusion thermo parameter (Du), Soret number or thermal diffusion parameter (Sr), Chemical reaction parameter (Kr), time (t) and decreasing with increasing values of Magnetic field parameter (M^2), Permeability parameter (K), Hall parameter (m), Prandtl number (Pr), Schmidt number (Sc), Angle of inclination parameter (α), Casson fluid parameter (γ), Rotation parameter (Ω) and Thermal radiation parameter (N).

- The influence of Grashof number for heat transfer (*Gr*), Grashof number for mass transfer (*Gc*), Magnetic field parameter (M^2), Permeability parameter (*K*), Hall parameter (*m*), Prandtl number (Pr), Schmidt number (*Sc*), Angle of inclination parameter (α), Casson fluid parameter (γ), Rotation parameter (Ω), Thermal radiation parameter (*N*), Dufour number or diffusion thermo parameter (*Du*), Soret number or thermal diffusion parameter (*Sr*), Chemical reaction parameter (*Kr*) and time (*t*) on skin-friction coefficient (Cf_2) due to secondary velocity profiles is discussed in tables 4, 5 and 6. From these tables, we observed that the skin-friction coefficient is increasing with increasing values of Grashof number for heat transfer (*Gr*), Grashof number for mass transfer (*Gc*), Magnetic field parameter (M^2), Permeability parameter (*K*), Hall parameter (*m*), Rotation parameter (Ω), Dufour number or diffusion thermo parameter (*Du*), Soret number or thermal diffusion parameter (*Sr*), Chemical reaction parameter (*Kr*), time (*t*) and decreasing with increasing values of Prandtl number (Pr), Schmidt number (*Sc*), Angle of inclination parameter (α), Casson fluid parameter (γ), and Thermal radiation parameter (*N*).
- The influence of Prandtl number (Pr), Thermal radiation parameter (*N*), Dufour number or diffusion thermo parameter (*Du*) and time (*t*) on rate of heat transfer coefficient or Nusselt number coefficient (*Nu*) due to temperature profiles is discussed in table 7. From this table, we observed that the rate of heat transfer coefficient is increasing with increasing values of Dufour number or diffusion thermo parameter (*Du*), time (*t*) and decreasing with increasing values of Prandtl number (Pr), Thermal radiation parameter (*N*).

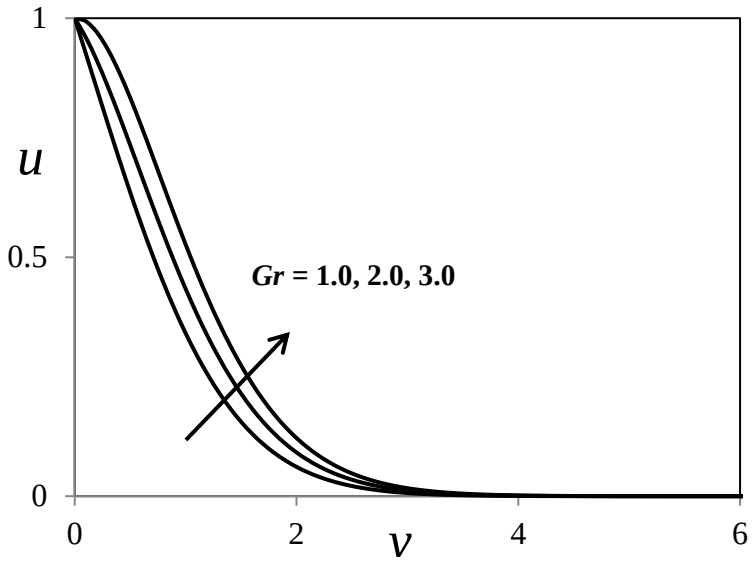

Fig. 3. *Gr* influence on primary velocity profiles

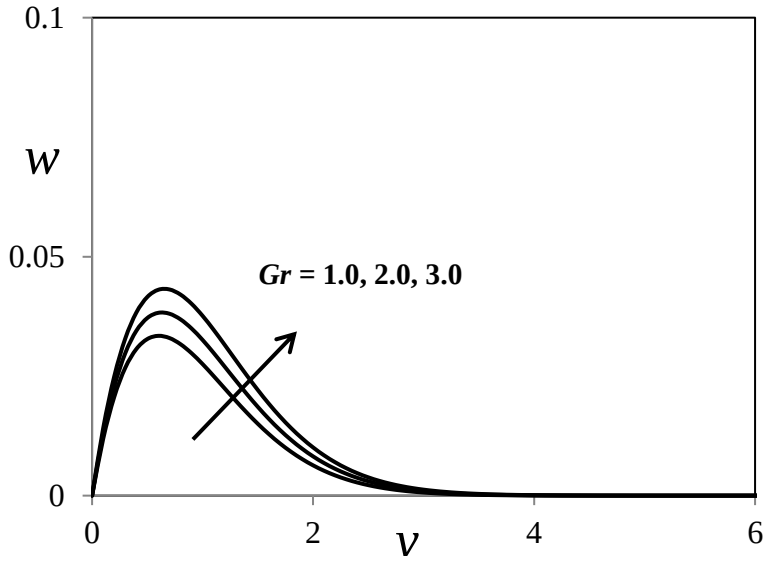

Fig. 4. *Gr* influence on secondary velocity profiles

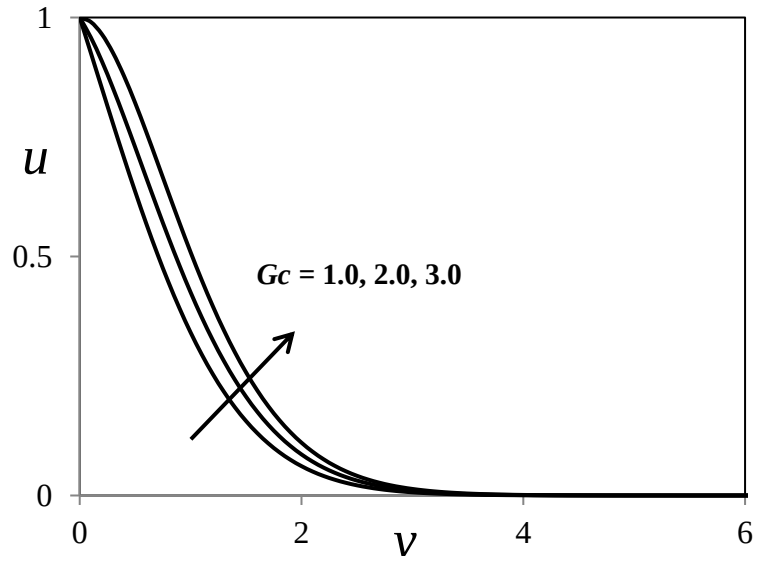

Fig. 5. *Gc* influence on primary velocity profiles

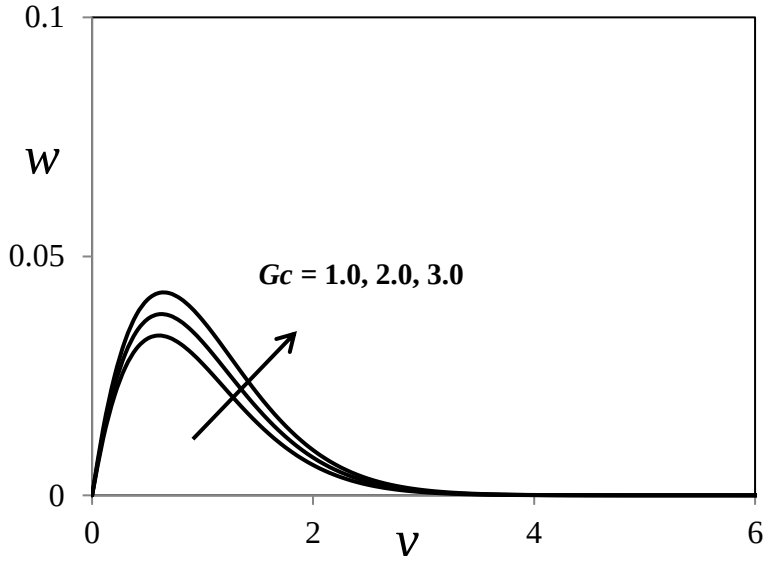

Fig. 6. *Gc* influence on secondary velocity profiles

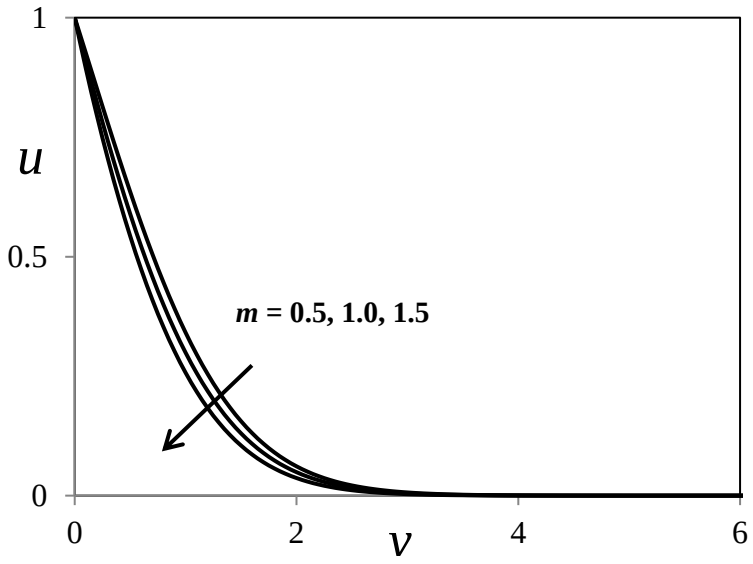

Fig. 7. *m* influence on primary velocity profiles

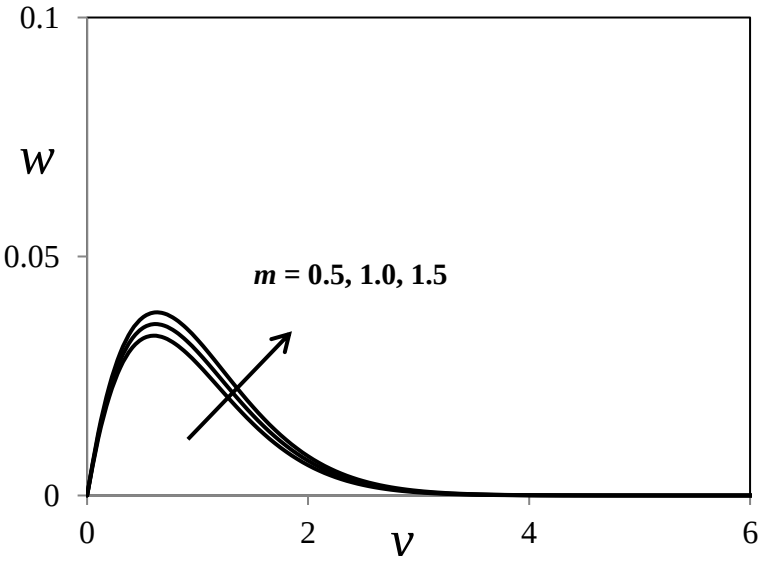

Fig. 8. *m* influence on secondary velocity profiles

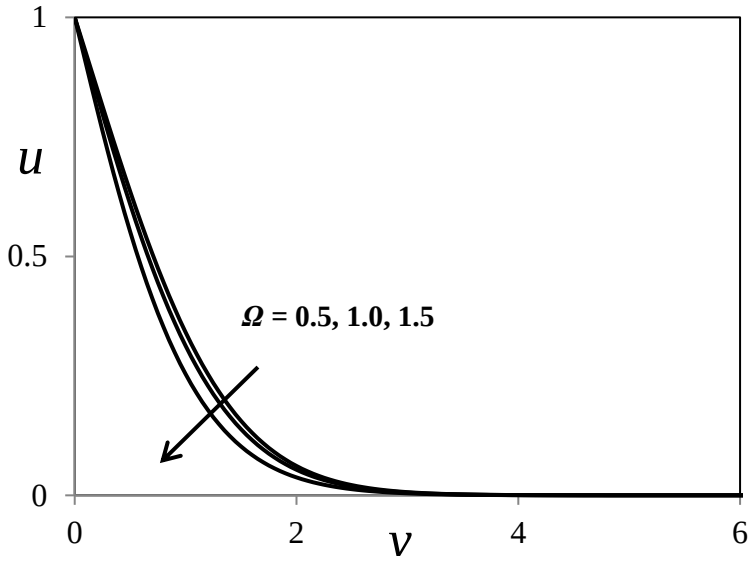

Fig. 9. *Ω* influence on primary velocity profiles

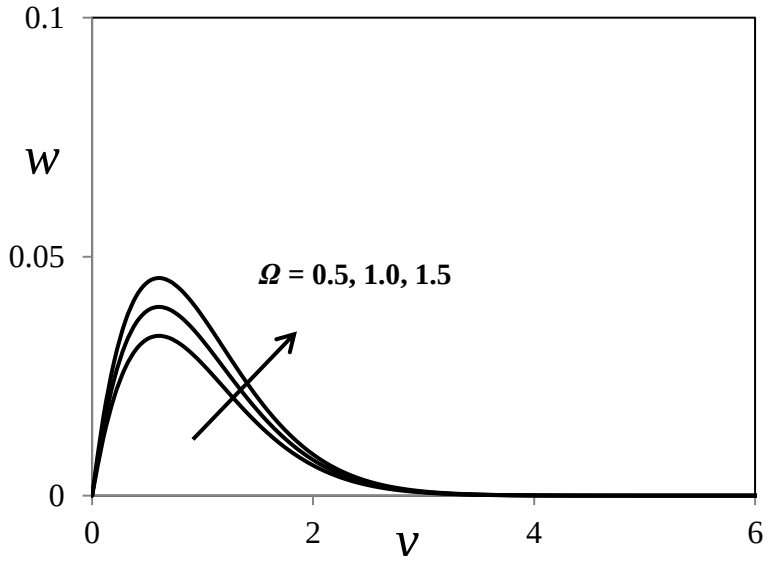

Fig. 10. *Ω* influence on secondary velocity profiles

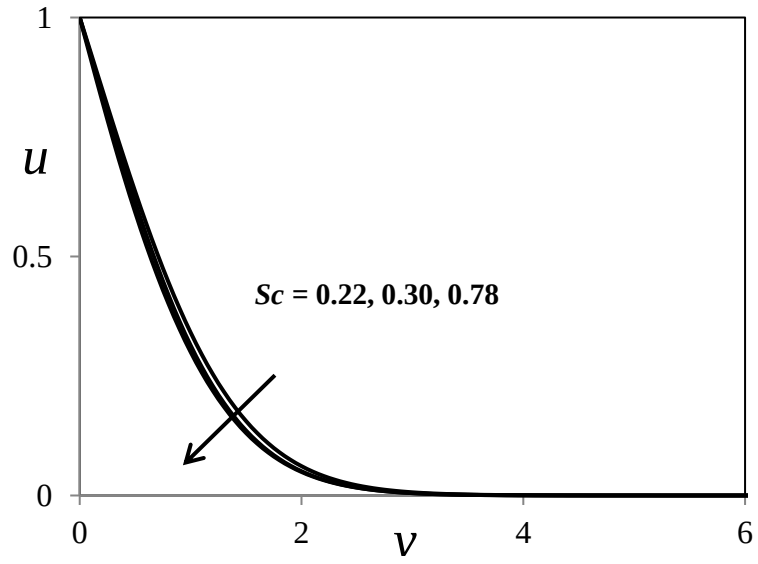

Fig. 11. *Sc* influence on primary velocity profiles

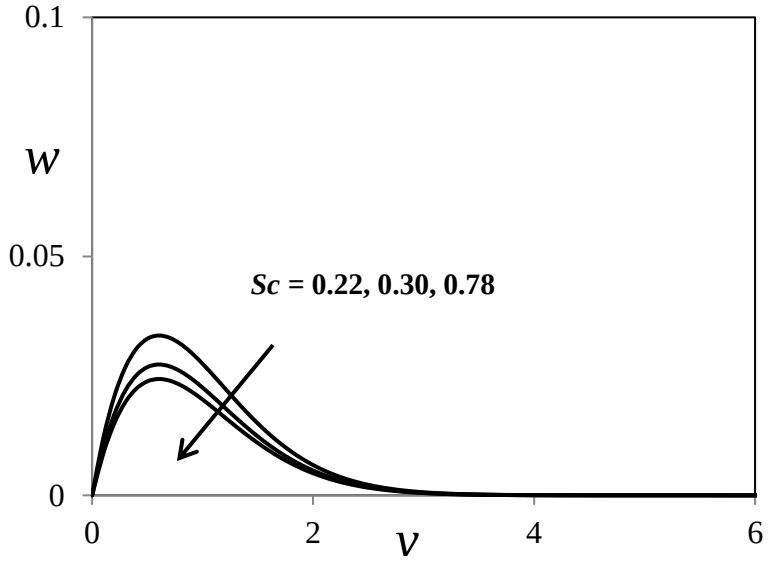

Fig. 12. *Sc* influence on secondary velocity profiles

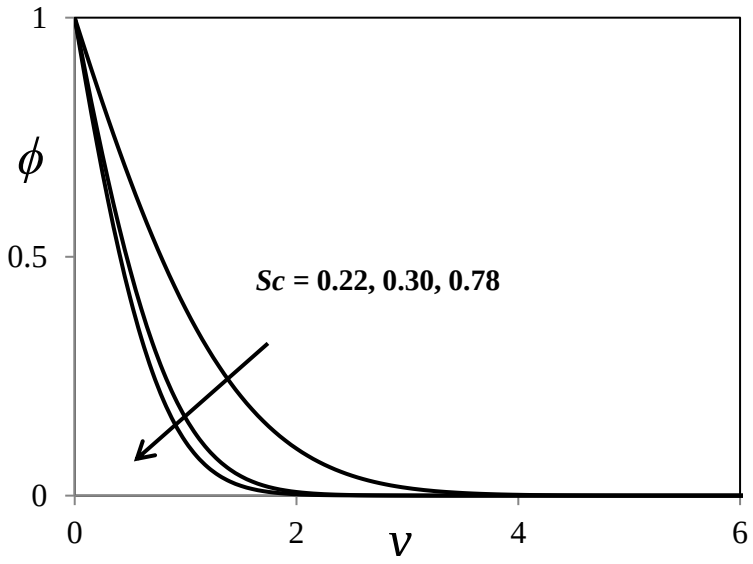

Fig. 13. *Sc* influence on concentration profiles

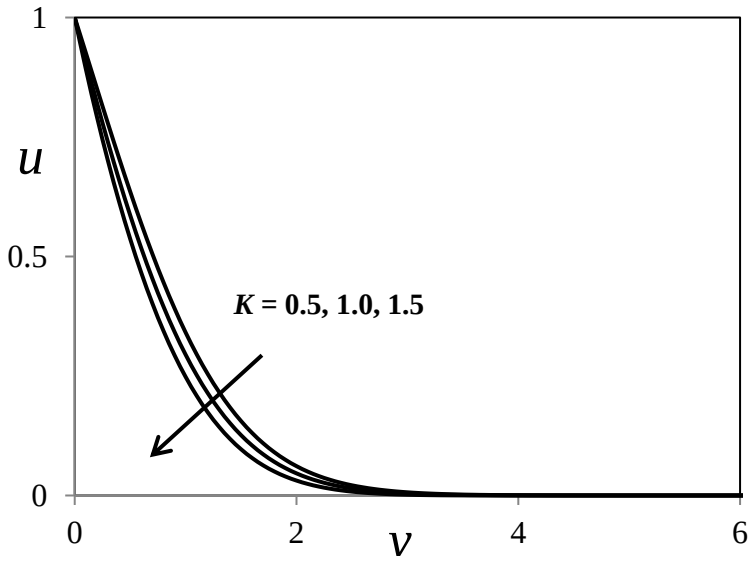

Fig. 14. *K* influence on primary velocity profiles

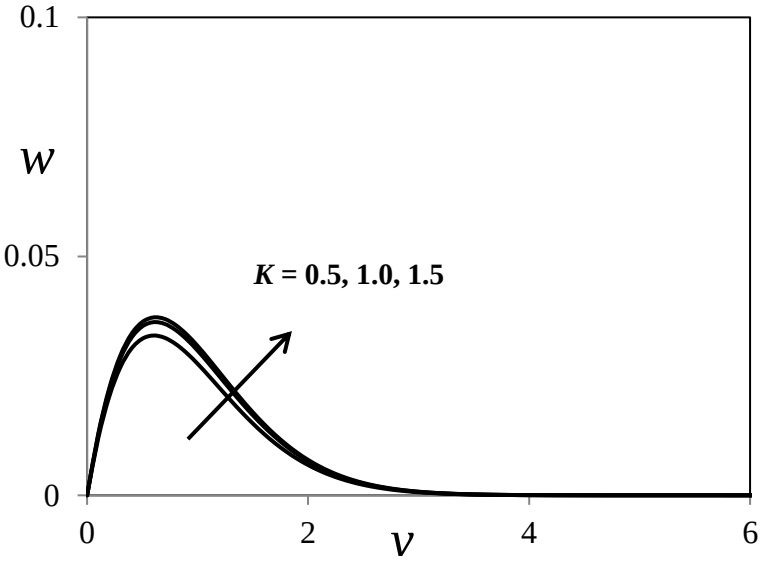

Fig. 15. *K* influence on secondary velocity profiles

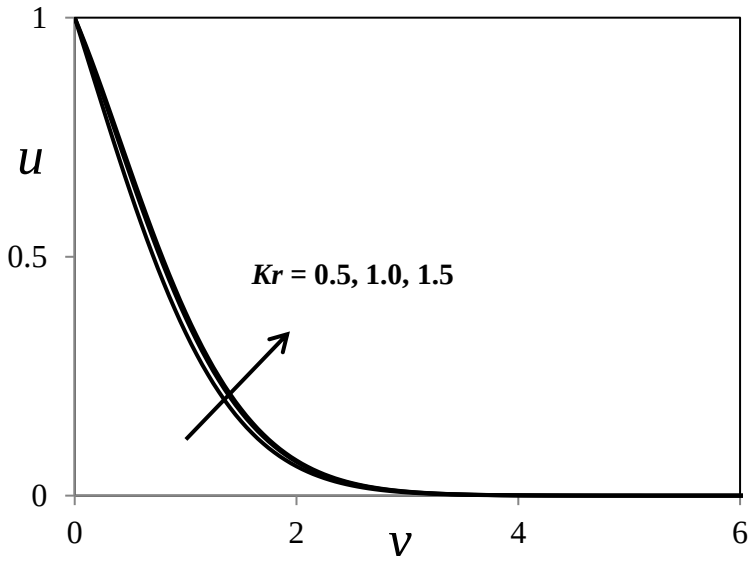

Fig. 16. *Kr* influence on primary velocity profiles

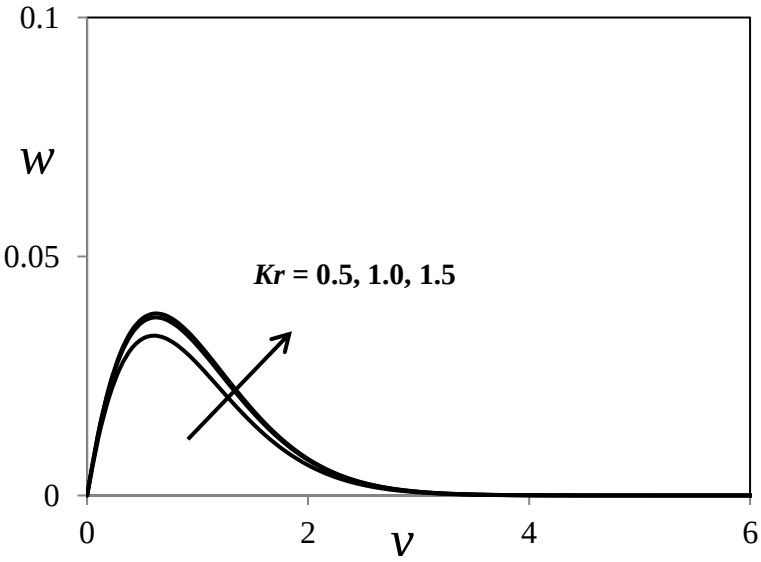

Fig. 17. *Kr* influence on secondary velocity profiles

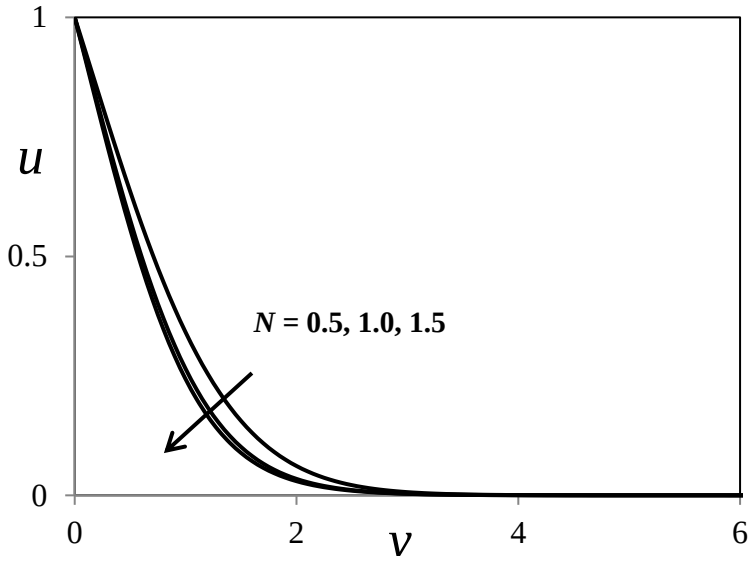

Fig. 18. *N* influence on primary velocity profiles

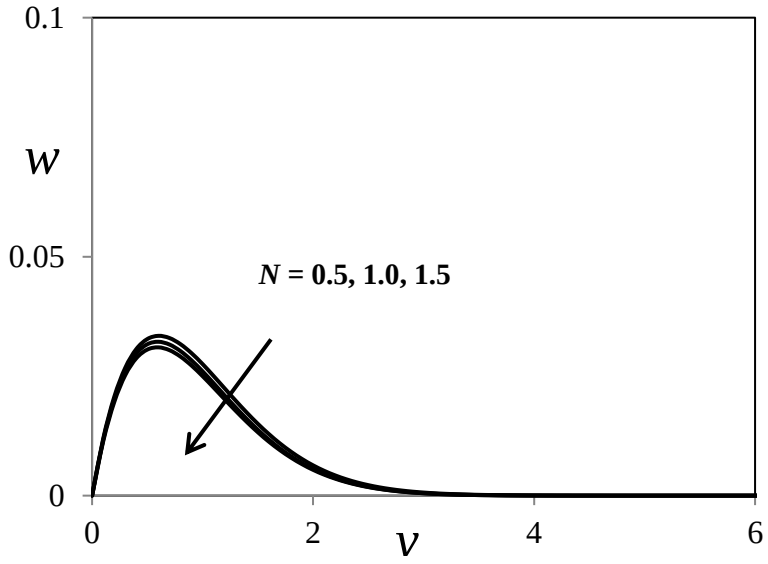

Fig. 19. *N* influence on secondary velocity profiles

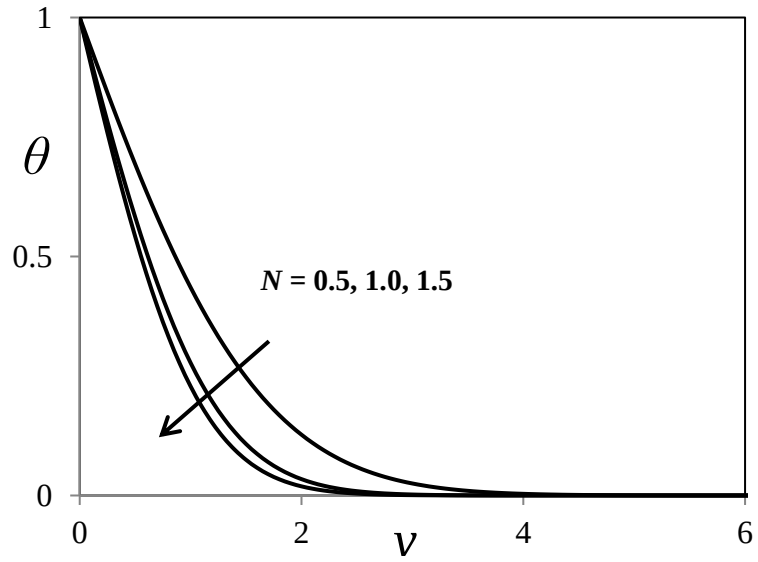

Fig. 20. *N* influence on temperature profiles

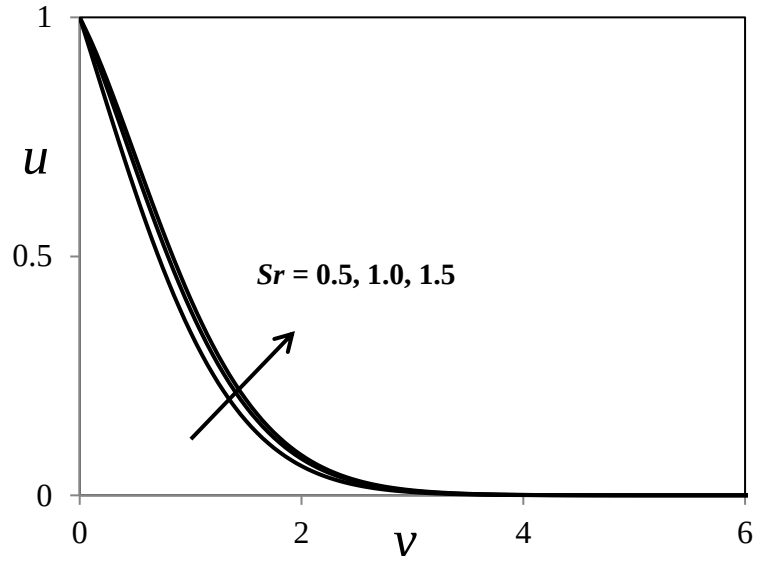

Fig. 21. *Sr* influence on primary velocity profiles

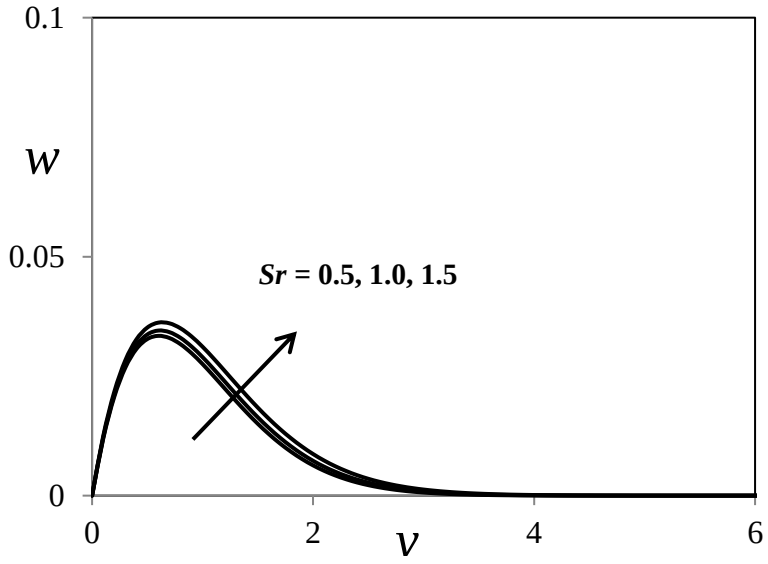

Fig. 22. *Sr* influence on secondary velocity profiles

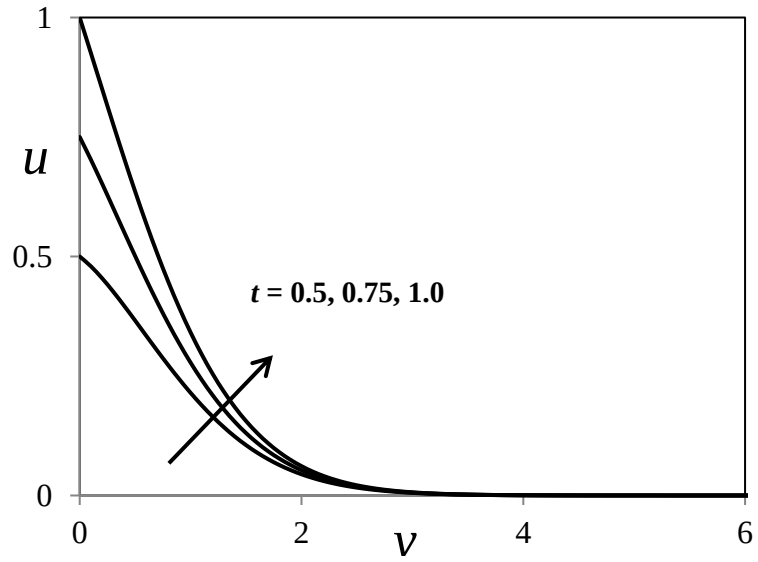

Fig. 23. *t* influence on primary velocity profiles

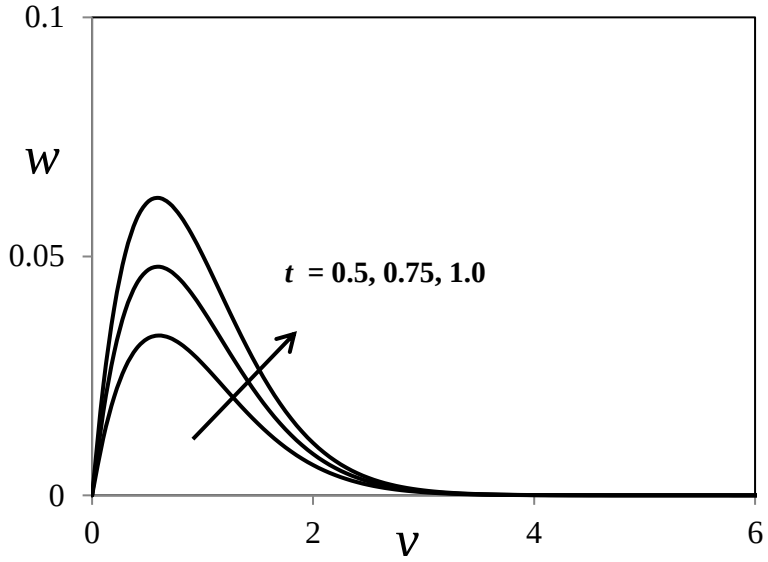

Fig. 24. *t* influence on secondary velocity profiles

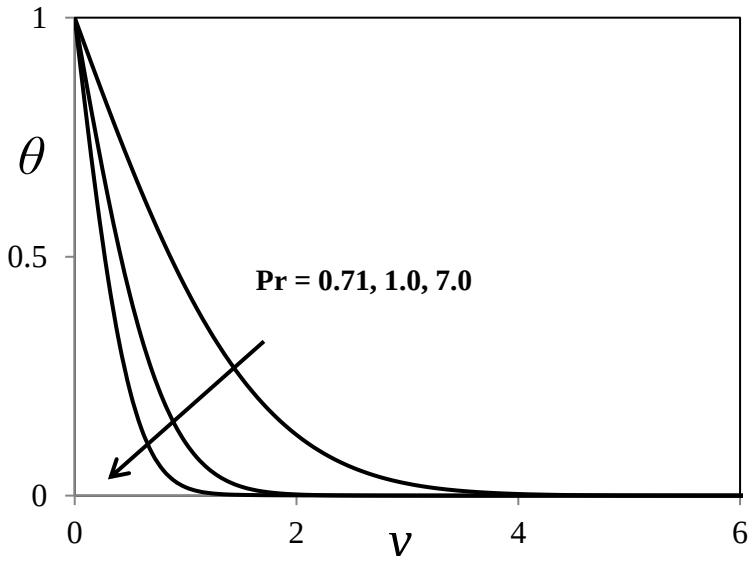

Fig. 25. Pr influence on temperature profiles

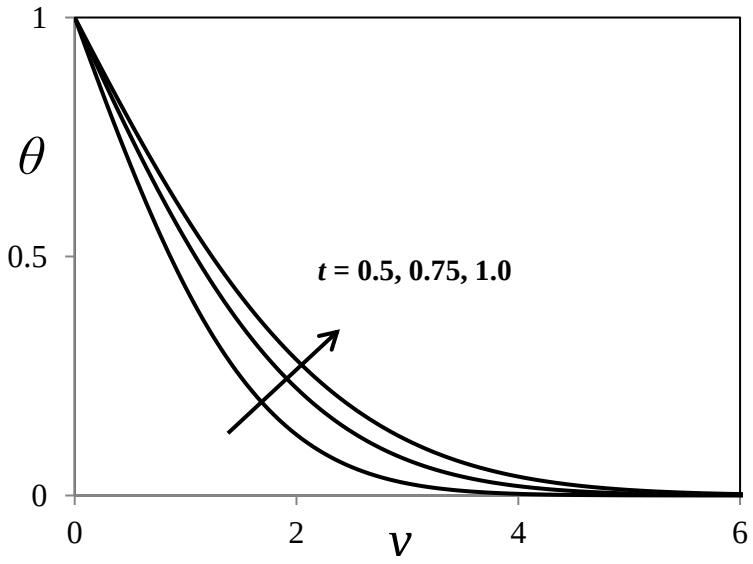

Fig. 26. *t* influence on temperature profiles

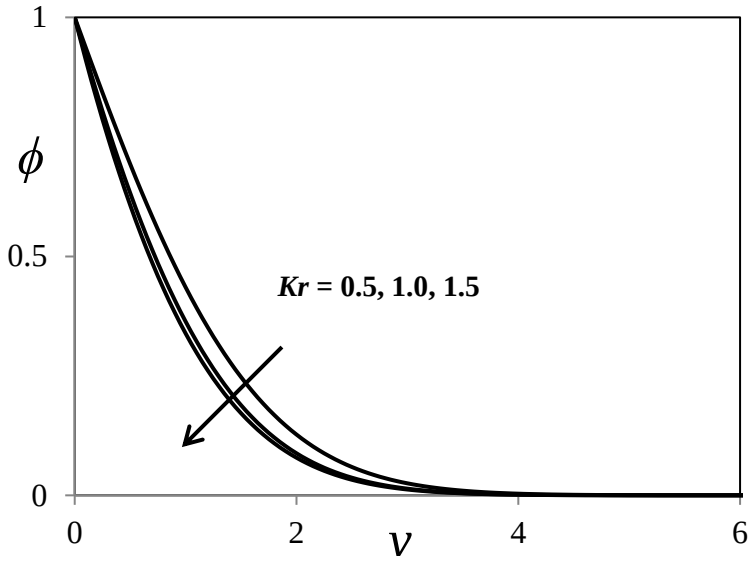

Fig. 27. *Kr* influence on concentration profiles

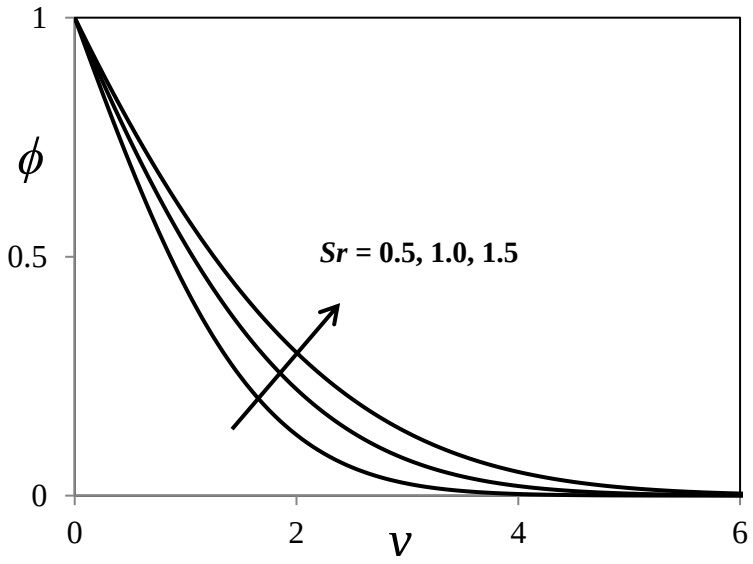

Fig. 28. *Sr* influence on concentration profiles

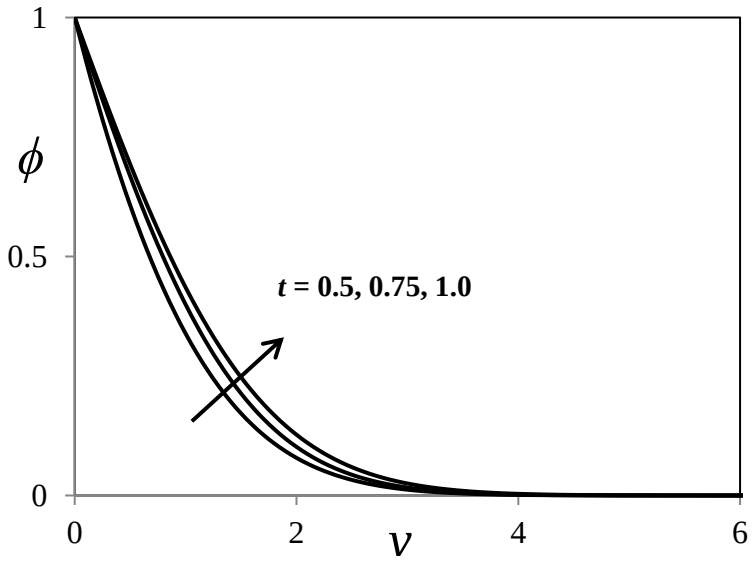

Fig. 29. *t* influence on concentration profiles

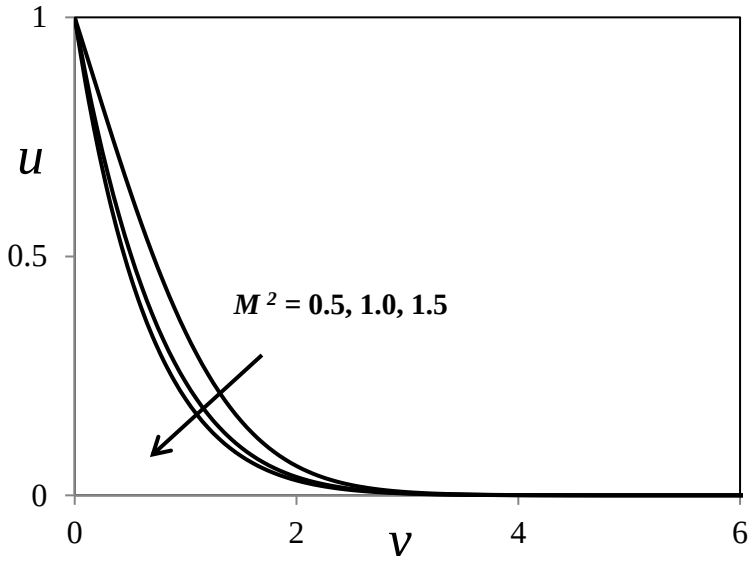

Fig. 30. M^2 influence on primary velocity profiles

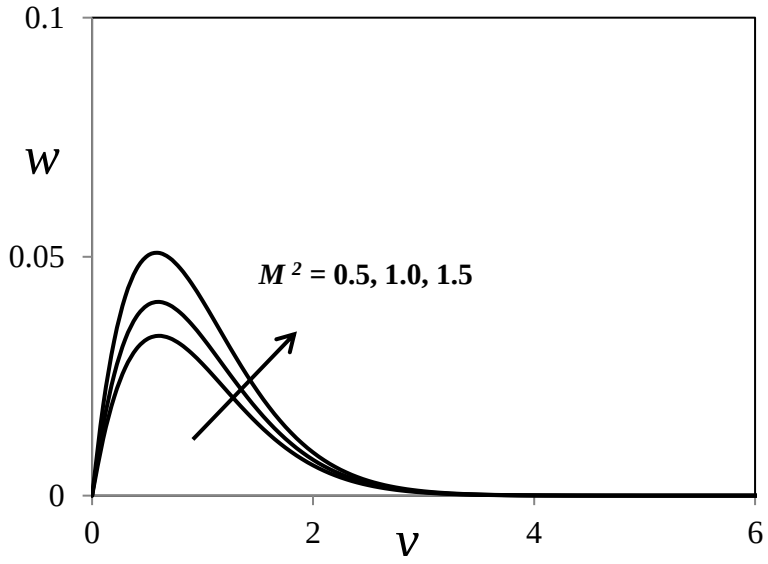

Fig. 31. M^2 influence on secondary velocity profiles

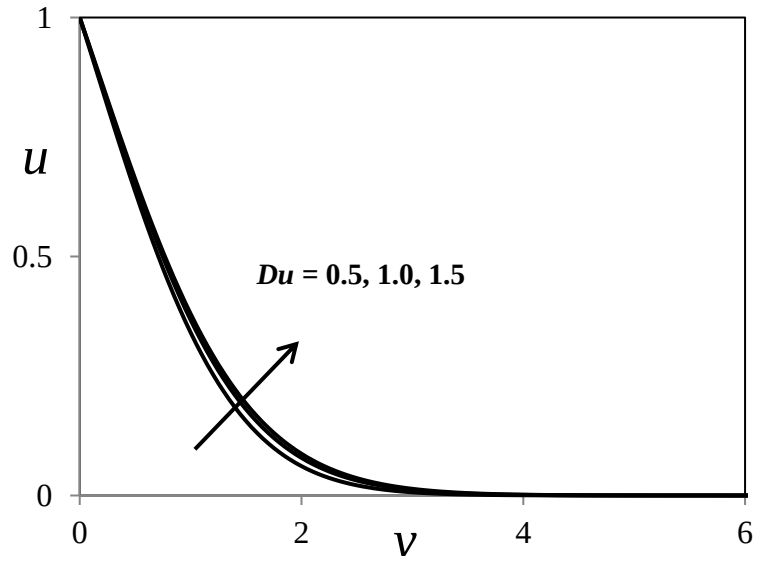

Fig. 32. *Du* influence on primary velocity profiles

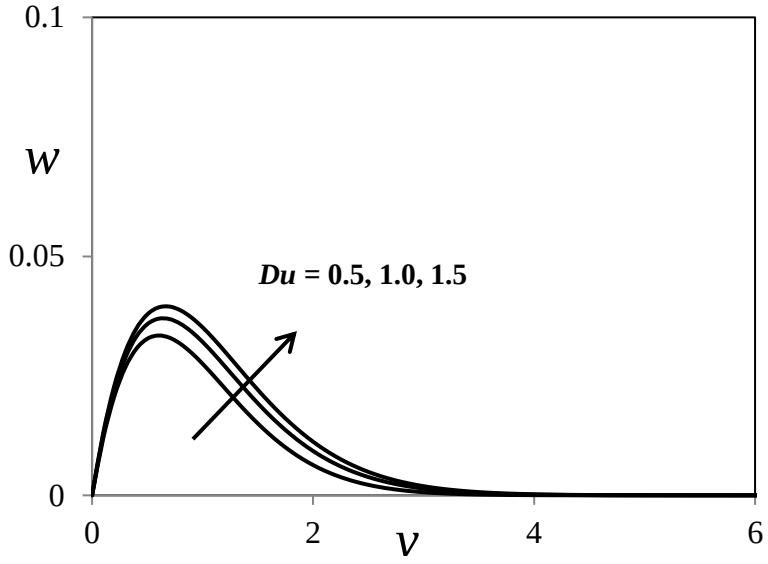

Fig. 33. *Du* influence on secondary velocity profiles

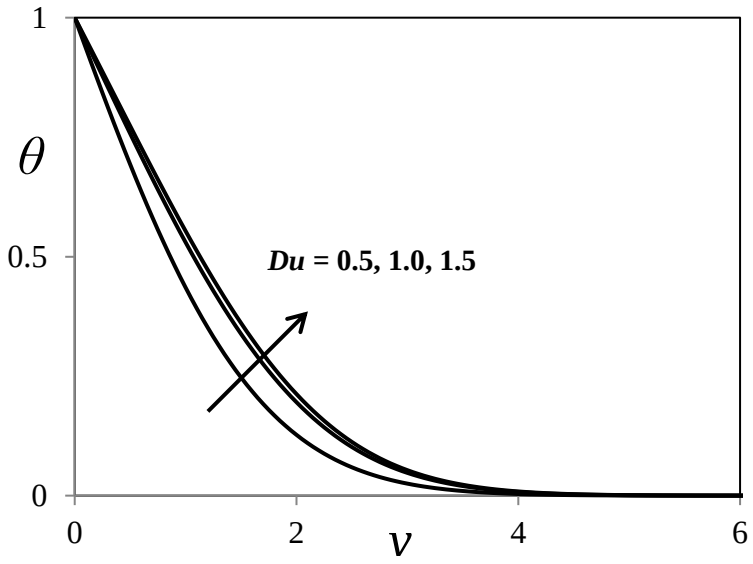

Fig. 34. *Du* influence on temperature profiles

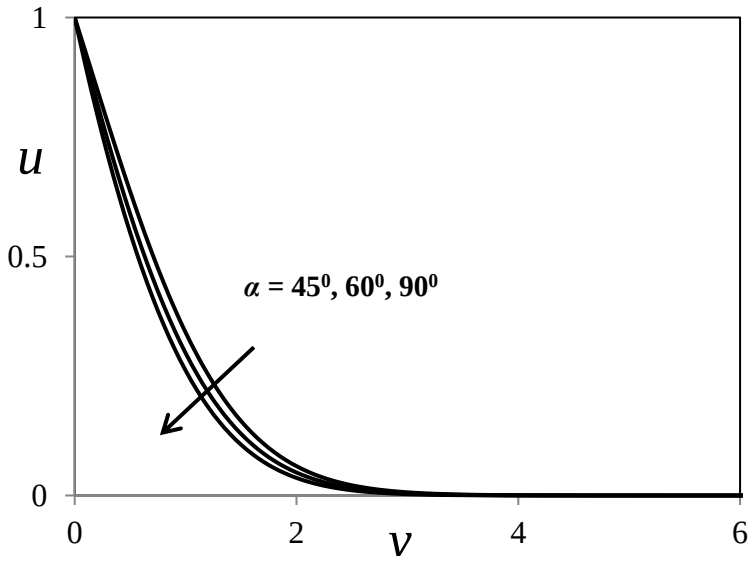

Fig. 35. *α* influence on primary velocity profiles

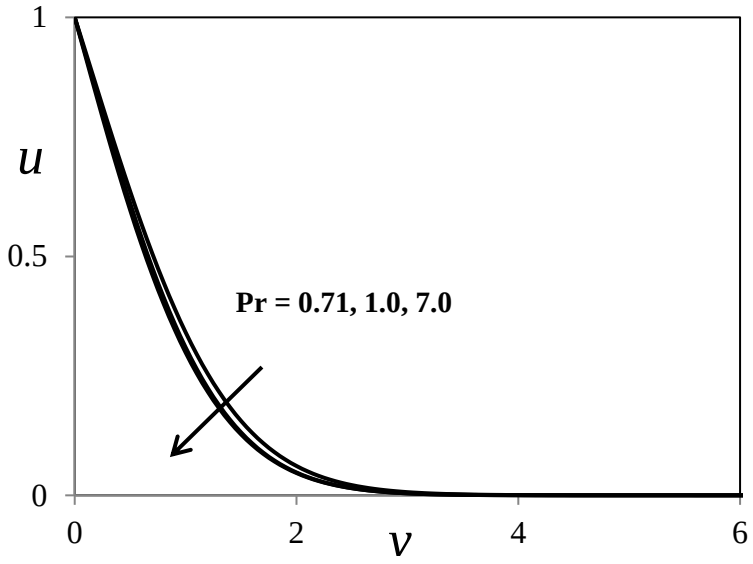

Fig. 36. Pr influence on primary velocity profiles

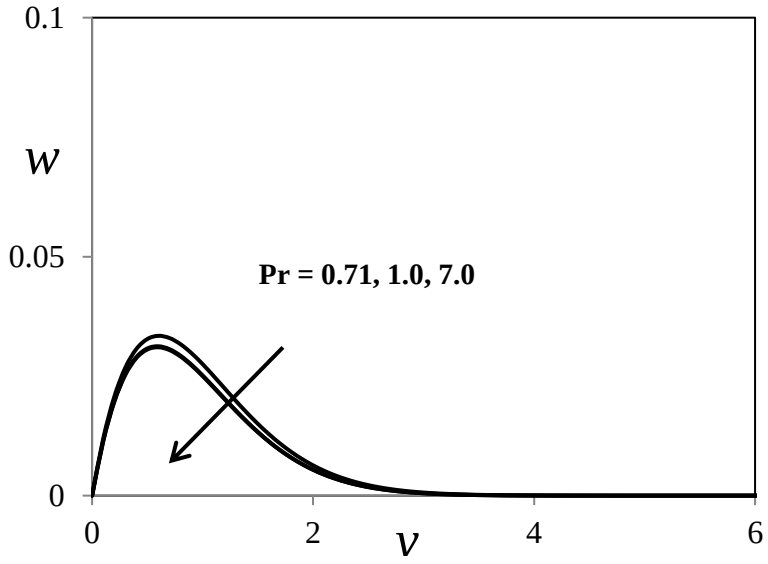

Fig. 37. Pr influence on secondary velocity profiles

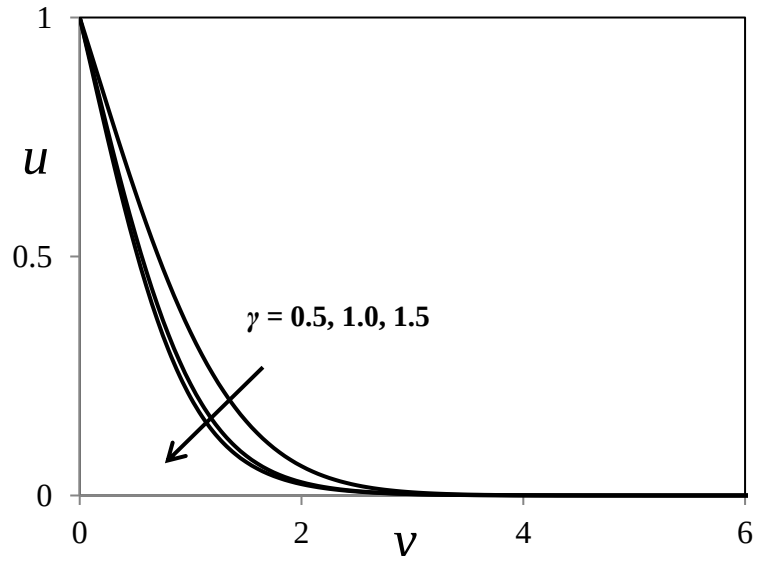

Fig. 38. γ influence on primary velocity profiles

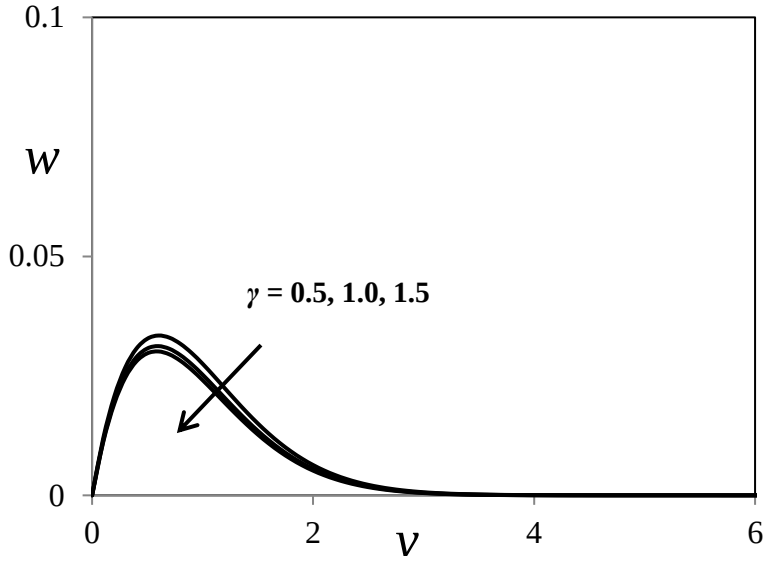

Fig. 39. γ influence on secondary velocity profiles

Table-1.: Numerical values of Skin-friction coefficient (Cf_1) due to primary velocity profiles for different values of *Gr*, *Gc*, M^2, *K* and *m*

Gr	*Gc*	M^2	*K*	*m*	Cf_1
1.0	1.0	0.5	0.5	0.5	0.9511248956
2.0	1.0	0.5	0.5	0.5	1.1022548651
1.0	2.0	0.5	0.5	0.5	1.1655202113
1.0	1.0	1.0	0.5	0.5	0.7551322649
1.0	1.0	0.5	1.0	0.5	0.8551233265
1.0	1.0	0.5	0.5	1.0	0.8777411152

Table-2.: Numerical values of Skin-friction coefficient (Cf_1) due to primary velocity profiles for different values of γ, α, Pr, *N* and *Du*

γ	α	Pr	*N*	*Du*	Cf_1
0.5	45^o	0.71	0.5	0.5	0.9511248956
1.0	45^o	0.71	0.5	0.5	0.8115622641
0.5	90^o	0.71	0.5	0.5	0.8666154892
0.5	45^o	7.00	0.5	0.5	0.7222195447
0.5	45^o	0.71	1.0	0.5	0.8661117853
0.5	45^o	0.71	0.5	1.0	0.9998514703

Table-3.: Numerical values of Skin-friction coefficient (Cf_1) due to primary velocity profiles for different values of Ω, *Sc*, *Sr*, *Kr* and *t*

Ω	*Sc*	*Sr*	*Kr*	*t*	Cf_1
0.5	0.22	0.5	0.5	1.0	0.9511248956
1.0	0.22	0.5	0.5	1.0	0.8029777841
0.5	0.30	0.5	0.5	1.0	0.7412555588
0.5	0.22	1.0	0.5	1.0	0.9871522656
0.5	0.22	0.5	1.0	1.0	1.0532216594
0.5	0.22	0.5	0.5	2.0	1.1326458899

Table-4.: Numerical values of Skin-friction coefficient (Cf_2) due to secondary velocity profiles for different values of *Gr*, *Gc*, M^2, *K* and *m*

Gr	*Gc*	M^2	*K*	*m*	Cf_2
1.0	1.0	0.5	0.5	0.5	0.0541126598
2.0	1.0	0.5	0.5	0.5	0.0855124886
1.0	2.0	0.5	0.5	0.5	0.0911452043
1.0	1.0	1.0	0.5	0.5	0.0744158812
1.0	1.0	0.5	1.0	0.5	0.0658221548
1.0	1.0	0.5	0.5	1.0	0.0695213255

Table-5.: Numerical values of Skin-friction coefficient (Cf_2) due to secondary velocity profiles for different values of γ, α, Pr, *N* and *Du*

γ	α	Pr	*N*	*Du*	Cf_2
0.5	45^o	0.71	0.5	0.5	0.0541126598
1.0	45^o	0.71	0.5	0.5	0.0322154896
0.5	90^o	0.71	0.5	0.5	0.0541126598
0.5	45^o	7.00	0.5	0.5	0.0156248952
0.5	45^o	0.71	1.0	0.5	0.0254112589
0.5	45^o	0.71	0.5	1.0	0.0788521625

Table-6.: Numerical values of Skin-friction coefficient (Cf_2) due to secondary velocity profiles for different values of Ω, *Sc*, *Sr*, *Kr* and *t*

Ω	*Sc*	*Sr*	*Kr*	*t*	Cf_2
0.5	0.22	0.5	0.5	1.0	0.0541126598
1.0	0.22	0.5	0.5	1.0	0.0666592148
0.5	0.30	0.5	0.5	1.0	0.0255689001
0.5	0.22	1.0	0.5	1.0	0.0778511015
0.5	0.22	0.5	1.0	1.0	0.0655895587
0.5	0.22	0.5	0.5	2.0	0.0677851009

Table-7.: Numerical values of rate of heat transfer coefficient (*Nu*) due to temperature profiles for different values of Pr, *N*, *Du* and *t*

Pr	*N*	*Du*	*t*	*Nu*
0.71	0.5	0.5	1.0	0.3226589785
7.00	0.5	0.5	1.0	0.1156220158
0.71	1.0	0.5	1.0	0.2115621548
0.71	0.5	1.0	1.0	0.4566210355
0.71	0.5	0.5	2.0	0.6211548952

Table-8.: Numerical values of rate of mass transfer coefficient (*Sh*) due to concentration profiles for different values of *Sc*, *Sr*, *Kr* and *t*

Sc	*Sr*	*Kr*	*t*	Cf_2
0.22	0.5	0.5	1.0	0.4112156215
0.30	0.5	0.5	1.0	0.3100156215
0.22	1.0	0.5	1.0	0.5877412156
0.22	0.5	1.0	1.0	0.2665188952
0.22	0.5	0.5	2.0	0.6522132549

- The influence of Schmidt number (*Sc*), Soret number or thermal diffusion parameter (*Sr*), Chemical reaction parameter (*Kr*) and time (*t*) on rate of mass transfer coefficient or Sherwood number (*Sh*) due to concentration profiles is discussed in table 8. From this table, we observed that the rate of mass transfer coefficient is increasing with increasing values of time (*t*), Soret number or thermal diffusion parameter (*Sr*) and decreasing with increasing values of Schmidt number (*Sc*), Chemical reaction parameter (*Kr*).

5. Validation of Numerical Results:

This section describes the validation of present skin-friction coefficients due to primary and secondary velocity profiles for various pertinent parameters in absence of Casson fluid, Angle of inclination and Diffusion thermo parameters with the skin-friction coefficients of Sarma and Pandit [24]. This validation code is discussed and presented in tables 9 and 10. From these tables, we observed that our numerical results are coincide with the results of Sarma and Pandit [24].

Table-9.: Comparison of present skin-friction coefficient results (Cf_1*) due to primary velocity profiles with the skin-friction coefficient results (Cf_1) of Sarma and Pandit [24] in absence of Casson fluid, Angle of inclination and Diffusion thermo

Sc	*K*	*m*	*t*	Cf_1*	Cf_1
0.22	0.5	0.5	1.0	0.8841154895	0.8884
0.60	0.5	0.5	1.0	0.6178445158	0.6172
0.22	1.0	0.5	1.0	0.9155489526	0.9144
0.22	0.5	1.0	1.0	0.9478852165	0.9411
0.22	0.5	0.5	2.0	0.9668415215	0.9664

Table-10.: Comparison of present skin-friction coefficient results (Cf_2*) due to secondary velocity profiles with the skin-friction coefficient results (Cf_2) of Sarma and Pandit [24] in absence of Casson fluid, Angle of inclination and Diffusion thermo

Sc	*K*	*m*	*t*	Cf_2*	Cf_2
0.22	0.5	0.5	1.0	0.2258478546	0.2258
0.60	0.5	0.5	1.0	0.1054414895	0.1054
0.22	1.0	0.5	1.0	0.3998541215	0.3990
0.22	0.5	1.0	1.0	0.1859941245	0.1856
0.22	0.5	0.5	2.0	0.5278845165	0.5277

6. Conclusions:

The effects of the Hall current, the rotation and the parameter of Soret in the non-stationary MHD convection were investigated, where heat transfer and viscosity were incompressible, and the mass of the conductive fluid was incorporated into the semi-porous infinite vertically inclined plate. The numerical solutions of the ruling equation is obtained by the finite difference technique. A complete set of graphs of fluid velocity, fluid temperature and fluid concentration are provided and their dependence on certain physical parameters is discussed. The important results are the following:

- The Hall current tends to accelerate the velocity of the secondary fluid throughout the region of the boundary layer, while having an adverse effect on the velocity of the primary fluid throughout the region of the boundary layer.
- The rotation tends to accelerate the velocity of the secondary fluid along the boundary layer, whereas it is counterproductive to the velocity of the primary fluid throughout the region of the boundary layer.

- In the presence of a uniform magnetic field, increases in the strength of the applied magnetic field decelerated the fluid motion along the wall of the plate inside the boundary layer.
- The permeability of the porous medium tends to accelerate the velocity of the secondary fluid through the region of the boundary layer, while being counterproductive to the velocity of the primary fluid passing through the boundary layer region.
- The parameter of Soret tends to accelerate the velocities of the primary and secondary fluid throughout the region of the boundary layer.
- The velocities of the primary and secondary fluid accelerate as time progresses along the region of the boundary layer.
- Thermal diffusion and thermal radiation tend to delay the temperature of the fluid and increase the temperature of the fluid over time in the region of the boundary layer.
- The diffusion of heat and mass tends to retard the concentration of the species, and the concentration of the substance increases due to the increase in the number and time of Soret in the entire region of the boundary layer.
- Increasing chemical reaction parameter is to decrease concentration profiles.
- In absence of Casson fluid, Angle of inclination and Diffusion thermo, the coefficients of skin-friction are in good agreement with the results of Sarma and Pandit [24].

7. Nomenclature:

List of variables:

B_o Intensity of the applied magnetic field ($A\ m^{-1}$)

C' Dimensionless species concentration of the fluid ($Kg\ m^{-3}$)

C_p Specific heat at constant pressure ($J\ Kg^{-1}K$)

C'_w Concentration in the fluid at the plate ($Kg\ m^{-3}$)

C'_∞ Concentration in the fluid far away from the plate ($Kg\ m^{-3}$)

D Chemical molecular diffusivity ($m^2\ s^{-1}$)

Gr Grashof number for heat transfer

Gc Grashof number for mass transfer

Pr Prandtl number

Sc Schmidt number

Kr Chemical reaction parameter

T' Temperature of the fluid (K)

T'_w Temperature of the plate (K)

T'_∞ Fluid temperature far away from the plate (K)

t Time (s)

u Velocity component in $x'-$direction ($m\ s^{-1}$)

U_o Reference velocity ($m\ s^{-1}$)

w Velocity component in $z'-$direction ($m\ s^{-1}$)

g Acceleration due to gravity ($m\ s^{-2}$)

K Permeability of the porous medium

M^2 Magnetic field parameter

m Hall parameter

Nu Rate of heat transfer coefficient (or) Nusselt number

Sh Rate of mass transfer coefficient (or) Sherwood number

N Thermal radiation parameter

Cf_1 Skin-friction coefficient due to primary velocity profiles

Cf_2 Skin-friction coefficient due to secondary velocity profiles

y Dimensionless coordinate (m)

q_r Radiative heat flux

x', y', z' Cartesian coordinates

u' Dimensional velocity component in $x'-$direction ($m\ s^{-1}$)

w' Dimensional velocity component in $z'-$direction ($m\ s^{-1}$)

K' Dimensional Permeability of the porous medium

K_r' Dimensional Chemical reaction parameter

t' Dimensional time (s)

Re Reynold's number

$\overline{B}$ Magnetic Induction Vector

$\overline{E}$ Electric field

$\overline{V}$ Velocity vector

$\overline{J}$ Electric current density vector

n_e Number of electron density

U Dimensionless plate translational Velocity ($m\ s^{-1}$)

Sr Soret Number (Thermal diffusion)

k_T Mean absorption coefficient

T_m Mean fluid temperature (K)

D_m Molecular diffusivity ($m^2\ s^{-1}$)

Du Dufour number (Diffusion thermo)

C_s Concentration susceptibility ($m\ mole^{-1}$)

Greek symbols:

β Coefficient of Volume expansion $\left(K^{-1}\right)$

ρ Density of the fluid $\left(kg/m^{-3}\right)$

β^* Volumetric Coefficient of expansion with Concentration ($m^3\ Kg^{-1}$)

ν Kinematic Viscosity $\left(m^2 s^{-1}\right)$

τ_x' Shear stress along $x'-$direction (N/m^2)

τ_z' Shear stress along $z'-$direction (N/m^2)

Ω Angular frequency (*Hertz*)

Ω' Dimensional angular frequency (*Hertz*)

θ Dimensionless Temperature (K)

σ Electrical conductivity, ($\Omega^{-1}m^{-1}$)

κ Thermal conductivity, W/mK

γ Casson fluid parameter

ϕ Species concentration of the fluid at the plate ($Kg\ m^{-3}$)

α Angle of inclination ($\deg rees$)

Superscript:

$'$ Dimensionless properties

Subscripts:

p	At the plate
w	Conditions on the wall
∞	Free stream conditions

References:

1. *N. T. M. Eldabe, M. G. E. Salwa, Heat transfer of MHD non-Newtonian Casson fluid flow between two rotating cylinders, J Phys Soc Jpn, 64 (1995), pp. 41-64.*
2. *S. A. Shehzad, T. Hayat, M. Qasim, S. Asghar, Effects of mass transfer on MHD flow of a Casson fluid with chemical reaction and suction, Braz J Chem Eng, 30 (2013), pp. 187-195.*
3. *M. N. Tufail, A. S. Butt, A. Ali, Heat source/sink effects on non-Newtonian MHD fluid flow and heat transfer over a permeable stretching surface: Lie group analysis, Indian J Phys, 88 (2013), pp. 75-82, 10.1007/s12648-013-0376-3.*
4. *S. K. Nandy, Analytical solution of MHD stagnation-point flow and heat transfer of Casson fluid over a stretching sheet with partial slip, ISRN Thermodyn, 2013 (2013), Article 108264, 10.1155/2013/108264*
5. *S. Mukhopadhyay, Casson fluid flow and heat transfer over a nonlinearly stretching surface, Chin Phys, 27 (2013), pp. 074701-074705.*
6. *K. Vajravelu, S. Mukhopadhyay, R. A. V. Gorder, Casson fluid flow and heat transfer at an exponentially stretching permeable surface, J Appl Mech, 80 (2013), pp. 054502-054509.*
7. *S. Mukhophadhyay, K. Vajravelu, Diffusion of chemically reactive species in Cassona fluid flow over an unsteady permeable stretching surface, J Hydrodyn, 25 (2013), pp. 591-598.*
8. *M. H. Abolbashari, N. Freidoonimehr, M. M. Rashidi, Analytical modeling of entropy generation for Casson nano-fluid flow induced by a stretching surface, Adv Powder Tech, 26 (2) (2015), pp. 542-552.*
9. *M. B. Ashraf, T. Hayat, A. Alsaedi, Mixed convection flow of Casson fluid over a stretching sheet with convective boundary conditions and Hall effect, Boundary Value Prob, 2017 (2017), p. 137*
10. *A. S. Butt, M. N. Tufail, A. Alia, Three-dimensinal flow of a magnetohydrodynamic Casson fluid over an unsteady stretching sheet embedded into a porous medium, J Appl Mech Tech Phys, 57 (2016), pp. 283-292*
11. *M. I. Khan, M. Waqas, T. Hayat, A. Alsaedi, A comparative study of Casson fluid with homogeneous-heterogeneous reactions, J Coll Int Sci, 498 (2017), pp. 85-90.*
12. *G. S. Seth, R. Tripathi, M. K. Mishra, Hydromagnetic thin film flow of a Casson fluid in a non-Darcy porous medium with Joule dissipation and Navier's partial slip, Appl Math Mech, 38 (11) (2017), pp. 1613-1626.*

13. *A. S. Gupta, Hydromagnetic flow past a porous flat plate with Hall effects, Acta Mech, 22 (1975), pp. 281-287.*
14. *A. J. Chamkha, MHD-free convection from a vertical plate embedded in a thermally stratified porous medium with Hall effects, Appl Math Modell, 21 (1997), pp. 603-609.*
15. *H. S. Takhar, A. J. Chamkha, G. Nath, MHD flow over a moving plate in a rotating fluid with magnetic field, Hall currents and free stream primary velocity, Int J Eng Sci, 40 (13) (2002), pp. 1511-1527.*
16. *T. Hayat, Z. Abbas, S. Asghar, Effects of Hall current and heat transfer on rotating flow of a second grade fluid through a porous medium, Commun Nonlinear Sci Numer Simul, 13 (2008), pp. 2177-2192.*
17. *A. M. Saleem, M. A. E. Aziz, Effect of Hall currents and chemical reaction on hydromagnetic flow of a stretching vertical surface with internal heat generation/absorption, Appl Math Model, 32 (2008), pp. 1236-1254.*
18. *G. S. Seth, R. Sharma, S. Sarkar, Natural convection heat and mass transfer flow with Hall current, rotation, radiation and heat absorption past an accelerated moving vertical plate with ramped temperature, J Appl Fluid Mech, 8 (1) (2015), pp. 7-20.*
19. *G. S. Seth, R. Tripathi, R. Sharma, An analysis of MHD natural convection heat and mass transfer flow with Hall effects of a heat absorbing, radiating and rotating fluid over an exponentially accelerated moving vertical plate with ramped temperature, Bul Chem Commun, 48 (4) (2016), pp. 770-778.*
20. *S. M. Hussain, J. Jain, G. S. Seth, M. M. Rashidi, Free convective heat transfer with Hall effects, heat absorption and chemical reaction over an accelerated moving plate in a rotating system, J Magn Magn Mater, 422 (2017), pp. 112-123.*
21. *D. Pal, Hall current and MHD effects on heat transfer over an unsteady stretching permeable surface with thermal radiation, Comput Math Appl, 66 (2013), pp. 1161-1180.*
22. *P. Jain, R. C. Chaudhary, Hall effect on MHD mixed convection flow of a viscoelastic fluid past an infinite vertical porous plate with mass transfer and radiation, Ukr. J. Phys., 52 (10) (2007), pp. 1001-1010.*
23. *P. V. Satya Narayana, B. Venkateswarlu, S. Venkataramana, Effects of Hall current and radiation absorption on MHD micropolar fluid in a rotating system, Ain Shams Eng. J., 4 (2013), pp. 843-854.*
24. *D. Sarma, K. K. Pandit, Effects of Hall current, rotation and Soret effects on MHD free convection heat and mass transfer flow past an accelerated vertical plate through a porous medium, Ain Shams Eng. J., 9 (2018), pp. 631-646.*
25. *T. G. Cowling, Magnetohydrodynamics. New York: Interscience Publishers, 1957.*

26. *K. R. Cramer, S. I. Pai, Magnetofluid dynamics for engineers and applied physicists. New York: McGraw Hill Book Company, 1973.*
27. *P. Sturdza, An aerodynamic design method for supersonic natural laminar flow aircraft Ph. D. thesis. California, USA: Dept. Aeronautics and Astronautics, Stanford University; 2003.*